Nationaal Lucht- en Ruimtevaartlaboratorium
National Aerospace Laboratory NLR

NLR-TP-2001-032

Microstructurally-induced embrittlement of archaeological silver

R.J.H. Wanhill

Nationaal Lucht- en Ruimtevaartlaboratorium
National Aerospace Laboratory NLR

NLR-TP-2001-032

Microstructurally-induced embrittlement of archaeological silver

R.J.H. Wanhill

This report has been prepared as a contribution to the archaeometallurgical literature.

Division: Structures and Materials
Issued: 22 January 2001
Classification of title: Unclassified

Contents

4 Tables, 11 Figures } Main text
2 Tables, 12 Figures } Appendices

(50 pages in total)

MICROSTRUCTURALLY-INDUCED EMBRITTLEMENT OF ARCHAEOLOGICAL SILVER

R.J.H. Wanhill
National Aerospace Laboratory NLR, Anthony Fokkerweg 2,
1059 CM Amsterdam, The Netherlands

ABSTRACT

Microstructurally-induced embrittlement of archaeological silver is characterized by grain boundary fracture. This is most likely due to impurity elements segregating to grain boundaries and reducing their cohesive strength. Empirical and theoretical concepts of segregation-induced embrittlement are considered with respect to silver and the impurity elements in archaeological silver, furthermore considering the special nature of grain boundaries and the influence of grain size. The report ends with surveys of diagnostic techniques and possible remedial measures for embrittled archaeological silver.

KEYWORDS: ARCHAEOLOGICAL SILVER, EMBRITTLEMENT, CRACKS, GRAIN BOUNDARIES, SEGREGATION, GRAIN SIZE, CORROSION, MICROSTRUCTURE, METALLOGRAPHY, FRACTOGRAPHY, RESTORATION, CONSERVATION, HEAT-TREATMENT, COATINGS

INTRODUCTION

Silver is normally malleable, ductile and easily fabricated. However, archaeological silver can be very brittle, as a long term consequence of corrosion and microstructural changes in the silver (Thompson and Chatterjee 1954; Werner 1965; Ravich 1993; Wanhill *et al*. 1998; Wanhill 2000a). This report considers microstructurally-induced embrittlement from current evidence, empirical and theoretical metallurgical concepts, and the chemical compositions of archaeological silver artifacts and coins. The report ends with surveys of diagnostic techniques and possible remedial measures for both microstructurally-induced and corrosion-induced embrittlement.

At this point it is opportune to distinguish between microstructurally-induced and corrosion-induced embrittlement. Microstructurally-induced embrittlement causes apparently pristine metal to crack and fracture under the action of external loads or forces. Corrosion-induced

embrittlement is a consequence of selective corrosion that penetrates the metal and eventually fragments it (Werner 1965; Ravich 1993; Wanhill *et al*. 1998) whether or not there are external loads or forces.

However, it is important to note that microstructurally-induced and corrosion-induced embrittlement can act synergistically, and that microstructural features are involved in both kinds of embrittlement (Wanhill *et al*. 1998; Wanhill 2000a).

EVIDENCE OF EMBRITTLEMENT

It has long been known that certain elements can embrittle silver, notably lead and tin (Ercker 1574) and antimony (Gowland 1918). The first detailed investigation appears to be due to Thompson and Chatterjee (1954). They studied the embrittlement of silver by age-hardening (age-embrittlement), prompted by the brittleness of archaeological silver coins that must have been ductile when struck.

Thompson and Chatterjee analysed fifteen brittle silver coins, finding copper and lead in appreciable quantities, but no other element except as a trace. The copper contents were up to several weight % and the lead contents varied from 0.25-1.6 wt. %. From these analyses they considered that embrittlement could be due to age-hardening owing to precipitation of lead from supersaturated solid solution in the silver matrix of Ag-Pb or Ag-Cu-Pb alloys. They provided evidence for this possibility as follows:

(1) By determining the silver-rich low temperature region of the Ag-Pb phase diagram, figure 1. This required weeks and months of ageing supersaturated solid solutions of lead in silver, and showed that a lead-rich phase (β) precipitates out of solution even at very low lead contents, less than 0.1 wt. %, and down to ambient temperatures.

(2) By mechanically testing age-hardened Ag-Pb and Ag-Cu-Pb alloys, figure 2, and showing that prolonged ageing led to brittle fracture.

However, lead-rich precipitates may not be necessary. Wanhill *et al*. (1998) examined a severely embrittled Egyptian silver vase, figure 3a. Microstructural embrittlement was characterized by “clean” grain boundary fracture with no sign of precipitates. This is illustrated in figure 3b, with the caveat that features on the grain boundary facets are due to localised corrosion after fracture. In view of the vase metal analysis (in weight %: 97.1 Ag-0.9 Cu-0.8 Au-0.7 Pb-0.3 Sb-0.2 Sn) and a theory of adsorption-induced embrittlement (Seah 1980a), Wanhill *et al*. concluded that embrittlement could have been due to lead atoms

segregating to grain boundaries and reducing their cohesive strength (Wanhill *et al*. 1998; Wanhill 2000a).

EMPIRICAL AND THEORETICAL METALLURGICAL CONCEPTS

The starting point for this part of the report is the observation that microstructurally-induced embrittlement and precipitation or segregation of impurity elements to grain boundaries are characteristic of elements having very low primary solid solubilities in the parent metal matrix (Seah 1980b; Shewmon 1998).

The topics to be considered are: primary solid solubility; equilibrium grain boundary segregation; grain boundary character; and alloy phase diagrams, non-equilibrium cooling and mechanical behaviour.

Primary solid solubility

Primary solid solubility is governed by atomic size differences between the solute and solvent and by the tendency to form intermediate phases and intermetallic compounds. These observations can be expressed, in order of importance, by the size-factor rule, the electrochemical differences and hence chemical affinities of the alloying components, and the electron concentration change upon alloying (Hume-Rothery and Raynor 1954; Pettifor 1984, 1988; Massalski 1996).

The size-factor rule states that when the atomic diameters of solute and solvent differ by more than 14-15 %, the size-factor is unfavourable and the primary solid solubility will generally be restricted to a few atomic per cent. It is, however, a negative rule: favourable size-factors do not necessarily mean high solid solubilities. Figure 4 illustrates the rule for solid solutions in silver. Rubidium, potassium and sodium have very unfavourable size-factors and, as table 1 shows, zero solid solubility. They are followed by lead, bismuth and thallium, with solid solubilities less than 8 at. %.

The next criterion, electrochemical difference and chemical affinity, is simply that the greater the electrochemical difference between solute and solvent, the greater is their affinity and tendency to form intermediate phases and intermetallic compounds. In turn, this means primary solid solubility will be restricted (Hume-Rothery and Raynor 1954; Massalski 1996). The electrochemical difference is quantifiable by differences in electronegativity of the alloying components (Pauling 1945, 1947; Darken and Gurry 1953; Gordy and Thomas 1956).

Much effort has been put into combining the size-factor rule and electronegativity differences on Darken-Gurry (D-G) maps, e.g. Darken and Gurry (1953), Waber *et al*. (1963), Gschneider (1980). D-G maps are supposed to enable predictions whether solid solubility is low or moderate-to-high. Figure 5 shows a D-G map for solid solutions in silver, using data from table 1. Solute elements outside the ellipse should have low solid solubilities, while elements within the ellipse are predicted to have solid solubilities greater than 5-10 at. %. However, again using table 1, we see that this latter prediction is incorrect with respect to tellurium. Also, lithium, palladium, arsenic and antimony are incorrectly predicted to have low solid solubility. These and other inadequacies of D-G maps have been explained by Gschneider (1980) in a general way, i.e. not specifically considering silver as the solvent. To overcome these inadequacies Gschneider presented several new rules, which he realised would make D-G maps largely unnecessary.

More recently, Pettifor (1984, 1988) derived a series of the elements that goes beyond electronegativity by also acknowledging the chemical similarity of elements from the same Group of the Periodic Table. Each element is given an empirical ordering number, and examples are given in table 1. Pettifor demonstrated the usefulness of this deceptively simple empirical approach by showing it enabled systematic separation of the crystal structures of many binary intermetallic compounds.

The third factor to consider is the electron concentration, which is the ratio of valence electrons to the number of atoms. Empirical studies of binary gold, silver and copper alloys, in particular with B-subGroup elements, have shown that when the effects of size-factor and electrochemical difference are “relatively small”, the primary solid solubility limits occur at fairly constant values of electron concentration (Hume-Rothery and Raynor 1954). In a famous theory, Jones (1937) provided an explanation of this phenomenon and derived a theoretical critical electron concentration of 1.41.

Figure 6 illustrates the electron concentration effect for binary silver alloys, whereby the solutes have favourable size-factors but the combination of electronegativity and chemical differences, expressed by Pettifor’s empirical ordering sequence, increases in going from cadmium to antimony. Most of the alloys have primary solid solubility limits at electron concentrations between 1.35-1.42, agreeing well with Jones’ theory. (However, this theory is known to have some problems (Cottrell 1988; Massalski 1996).)

Equilibrium grain boundary segregation

Equilibrium grain boundary segregation involves the solid state redistribution of solute elements and their adsorption at grain boundaries. Solutes of low solubility generally segregate strongly

and vice versa (Seah 1980b). Another important characteristic is that at the commonly observed levels of segregation many elements co-segregate rather than compete for grain boundary adsorption sites (Hondros and Seah 1977; Seah 1980b).

This type of segregation can greatly reduce the cohesive strength of grain boundaries, leading to grain boundary fracture and embrittlement (Seah 1980a, 1980b; Shewmon 1998), and Seah (1980a) has developed a theory of embrittlement owing to adsorption-induced grain boundary decohesion. Figure 7 shows the theory's predictions for segregant elements in silver. This figure should be interpreted as follows: elements with sublimation enthalpies lower than those of the matrix will, *if segregated*, cause embrittlement of the matrix grain boundaries, and the embrittling effect will be greater the lower the sublimation enthalpy of the segregant element. (The sublimation enthalpy is a measure of the heat required to evaporate atoms from the solid surface of an element.)

Figure 8 correlates alloying element primary solid solubility limits in silver with their sublimation enthalpies. The elements are arranged according to Pettifor's (1988) empirical ordering numbers and unfavourable size-factors are indicated. The shaded regions in this figure indicate the matrix and alloying element combinations that would seem most likely to result in segregation-induced grain boundary fracture under equilibrium conditions: silver containing sodium, potassium, rubidium, lead, bismuth, tellurium and selenium. There are other possibilities, namely silver containing thallium, germanium, antimony and arsenic.

However, the key question, unanswerable by figures 7 and 8, is whether the indicated alloying elements actually segregate to grain boundaries to cause embrittlement. Another important question is whether they might cause embrittlement in another way. To try to answer these questions, and also to explain the observed embrittlement of silver discussed earlier, it is necessary to consider the grain boundary characteristics of archaeological silver, the binary silver alloy phase diagrams, the effects of non-equilibrium cooling on the phase changes, and the likely mechanical behaviour of the alloys.

Grain boundary character

Grain boundaries strongly influence the properties of metals and alloys, and there is much evidence that grain boundaries have different properties depending on their character, i.e. their type and structure (e.g. McLean 1957; Chadwick and Smith 1976; Baluffi 1980; Watanabe 1984, 1993, 1994; Watanabe *et al*. 1980, 1989; Lim and Watanabe 1990).

From the literature and their own research Watanabe (1984, 1993, 1994) and Watanabe *et al*. (1980, 1989) suggested dividing grain boundaries into three character-determined categories: low-angle boundaries with misorientation angles less than 15°; high-angle coincidence boundaries with low Σ coincidence*; and high-angle random boundaries. The basic distinguishing property is that low-angle and low Σ coincidence boundaries are low-energy boundaries, while random boundaries are high-energy boundaries. This difference is important for many other properties, including impurity element segregation, which occurs preferentially to high-angle random grain boundaries (Watanabe *et al*. 1980). This is illustrated schematically in figure 9, which also shows – consistent with observations (Seah 1980b) – that segregation tends to be greater for impurity elements having less primary solid solubility.

This distinction between grain boundary types and structures is informative for microstructurally-induced embrittlement of archaeological silver artifacts. These were usually made using combinations of mechanical working and annealing heat-treatments. The resulting microstructures most probably contain a majority of high-angle random grain boundaries, see e.g. Watanabe (1984) and Watanabe *et al*. (1989). In turn, this suggests that archaeological silver artifacts contain many grain boundaries very susceptible to impurity element segregation, *if it has occurred*.

Furthermore, despite the presence of other types of grain boundary, the likely preponderance of high-angle random grain boundaries in archaeological silver artifacts means it is reasonable, and indeed consistent with empirical observations (Werner 1965), to apply a simple length scale criterion – based on the average grain size or diameter – to crack initiation. This is considered later in the report, in the main section discussing microstructurally-induced embrittlement.

Alloy phase diagrams, non-equilibrium cooling, and mechanical behaviour

Table 2 lists the equilibrium phase diagram characteristics and ambient temperature phases for dilute silver binary alloys whose alloying elements have low primary solid solubilities.

Phase changes for the alloys in sub-table 2.1 should be independent of cooling rate, within normal metallurgical variations. This basic independence of cooling rate means that in the as-cast condition there will always be intercrystalline or intergranular phases. These are usually

* Grain boundaries can be classified using the concept of a Coincident Site Lattice (CSL), see Gleiter (1996). A boundary is then defined according to the ratio of the volume of a unit cell of the CSL to the volume of a unit cell from the grains on either side of the boundary. This ratio is denoted by Σ. A low value of Σ implies many coincident sites (atom positions) per unit area of the boundary. Such boundaries are called low Σ coincidence boundaries.

brittle intermetallic compounds and cause poor mechanical behaviour. Evidence for this is provided by Roberts-Austen's experiments on binary gold alloys (Roberts-Austen 1888; Wanhill 2000b).

Phase changes for the alloys in sub-tables 2.2 and 2.3 will depend on cooling rate. This will be illustrated with the aid of figure 10, which shows schematic binary alloy equilibrium phase diagrams involving eutectic or peritectic reactions. Consider two dilute alloys whose bulk compositions approach the primary solid solubility limits, α_3, and are represented by the vertical lines meeting the abscissae at X. Non-equilibrium cooling has two major effects on the phase changes:

(1) If cooling is fast enough the solidification compositions follow the curves α_1–α_3' rather than α_1–α_3. This means the solid solubilities are reduced, final solidification is at temperatures T_3 instead of T_2, the last liquids to solidify have compositions L_3 instead of L_2, and the alloys do not finally solidify only as α. Instead the eutectic or peritectic reactions occur at T_3: the remaining liquids either solidify as eutectic $\alpha+\beta$ between the primary α crystals or grains, or else react – the peritectic reaction – with some of the primary α crystals or grains to form β between them.

(2) Suppression of solid state reactions and the retention of metastable phases down to ambient temperatures. This is possible because the diffusion of atoms is much slower in solids than in liquids. From figure 10 we see that under equilibrium conditions the two alloys undergo solid state partial decomposition ($\alpha \rightarrow \alpha+\beta$) at temperatures below T_4. However, faster cooling will cause supersaturated α to be retained, at least temporarily, down to ambient temperatures.

These effects may be interpreted to some extent for the alloys in sub-tables 2.2 and 2.3. Firstly, non-equilibrium cooling could cause alloys with bulk compositions below $PSSL_{max}$ or $PSSL_{eut}$ to finally solidify as though their bulk compositions were above these limits, leading to poor mechanical properties. *Indirect* evidence for this is the behaviour of gold containing thallium. In this system the solid solubility of thallium becomes zero well above the eutectic temperature, resulting in eutectic Au+Tl between the primary crystals or grains however dilute the alloy (Baker *et al*. 1992; Wanhill 2000b). Roberts-Austen (1888) noted the "crystalline structure" of the fracture surface of an as-cast Au-0.2 wt. % (≈ 0.2 at. %) Tl bar whose ductility was low.

Secondly, the solid state decomposition reactions listed in the last two columns of sub-tables 2.2 and 2.3 could be partially or wholly prevented by non-equilibrium cooling. Subsequent ageing at low or even ambient temperatures could then result, in some cases, in alloying element

segregation and precipitation, and mechanical behaviour deterioration and embrittlement. The archetype is provided by the Ag-Pb alloy experiments of Thompson and Chatterjee (1954), discussed in the previous main section of this report and illustrated by figures 1 and 2. Other – candidate – systems are silver containing arsenic, bismuth and thallium. On the other hand, the Ag-Sb and Ag-Sn systems are less likely to belong to this category, even though antimony and tin can embrittle silver (Ercker 1574; Gowland 1918). The reason is that the solid solubilities of antimony and tin in silver are still significant at ambient temperatures, see sub-table 2.2. Finally, the Ag-Ge system would appear to be excluded, since germanium has a higher sublimation enthalpy than silver, see table 1 and figures 7 and 8.

Summary

Empirical and theoretical metallurgical concepts enable specifying which elements, in amounts less than about 5 at. %, could embrittle or impair the mechanical behaviour of silver. There are two categories, alloys most probably embrittled as-cast, and alloys that could be embrittled by low temperature ageing that results in alloying element segregation and precipitation. These categories are given below, whereby asterisks indicate known embrittlement or poor mechanical behaviour of dilute alloys (Thompson and Chatterjee 1954; Raub 1995):

(1) As-cast : Ag-Bi, Ag-Na, Ag-Pb, Ag-Rb, Ag-Se, Ag-Te*.

(2) Aged : Au-As, Ag-Bi, Ag-Pb*, Ag-Tl.

For both categories the presence of more than one of the specified elements could be cumulatively detrimental. This is probable for aged alloys in which impurity elements have segregated to grain boundaries since, as remarked earlier, many elements co-segregate rather than compete for grain boundary adsorption sites.

For archaeological silver only the second category – aged alloys – is likely to be relevant. Most artifacts were made by subjecting buttons or ingots with as-cast microstructures to mechanical working and intervening annealing heat-treatments. As-cast embrittlement could not have been tolerated: the silver would have been reprocessed until malleable and ductile. By the same token, however, the microstructures of most artifacts should contain many grain boundaries very susceptible to impurity element segregation owing to low temperature ageing.

COMPOSITION OF ARCHAEOLOGICAL SILVER

Native silver alloys may or may not have been used for Old World archaeological artifacts (Lucas 1928; Gale and Stos-Gale 1981a; Philip and Rehren 1996). However, the general scarcity of native silver compared to silver-containing minerals, mostly lead ores, and the early development of lead cupellation resulted in pyrometallurgy becoming the main source of silver (Gowland 1918; Gale and Stos-Gale 1981a, 1981b; Tylecote 1986; Raub 1995).

Cupellation is very effective in producing silver above 95 wt. % purity (Tylecote 1986, 1987), though it usually contains minor-to-trace amounts of gold, copper, lead and bismuth, and traces of antimony, arsenic, tellurium, zinc and nickel (McKerrell and Stevenson 1972; Gale and Stos-Gale 1981a; Raub 1995). Gold, copper, lead and bismuth contents are generally below 1 wt. % for each element: higher copper and lead contents in finished artifacts and coins, and also tin or zinc above 0.1 wt. %, suggest or indicate deliberate alloying, see McKerrell and Stevenson (1972) and Gale and Stos-Gale (1981a).

Figure 11 quantifies actually or potentially embrittling elements found in archaeological silver artifacts and coins lying within two ranges of high silver content. Though there are wide variations, lead is the main impurity, averaging 0.5-1 wt. %. Bismuth, antimony and tin are generally below 0.5 wt. %.

DISCUSSION OF MICROSTRUCTURALLY-INDUCED EMBRITTLEMENT

Description and mechanism

Microstructurally-induced embrittlement of archaeological silver appears to be entirely intergranular. The cracks are characteristically narrow and sharp (Wanhill 2000a) except where grains can become bodily displaced, e.g. figure 3b, which is itself a characteristic of severe embrittlement. Also, there is no evidence of plastic deformation of the grain boundaries (see figure 3b and Wanhill *et al*. 1998; Wanhill 2000a) unlike that occurring in the vicinity of low-energy boundaries (Watanabe 1984).

The evidence and empirical and theoretical concepts point to a mechanism of embrittlement by long-term low temperature ageing, whereby segregation of an impurity element, or elements, occurs to grain boundaries. The candidate impurity elements are arsenic, bismuth, lead, thallium and – less likely – antimony and tin.

Lead is the most likely perpetrator. This is inferred from the long-term ageing experiments and brittle coin analyses by Thompson and Chatterjee (1954); the Egyptian vase investigated by Wanhill *et al.* (1998), which contained lead, antimony and tin, but no detectable arsenic or bismuth; and the impurity element contents of many artifacts and coins, figure 11, where it is seen that lead is the main impurity. However, embrittlement by other impurity elements – notably bismuth, see figure 8 – is possible, especially in co-segregating action with lead.

Influence of grain boundary character and grain size

As indicated earlier in this report, microstructurally-induced embrittlement should mostly affect high-angle random grain boundaries (Watanabe *et al*. 1980; Watanabe 1984), which very likely predominate in the microstructures of archaeological silver artifacts. This has two important implications:

(1) Archaeological silver artifacts contain many grain boundaries very susceptible to impurity element segregation and microstructurally-induced embrittlement, *if it has occurred*.

(2) It is reasonable to try to describe embrittlement using a length scale criterion based on the average grain size or diameter, even though such criteria assume implicitly that all grain boundaries are the same.

Archaeological silver may have large grain sizes, more than 0.1 mm (e.g. Werner 1965; Wanhill *et al*. 1998). This is because the annealing heat-treatments usually involved in artifact manufacture were more or less uncontrolled, and the metalsmith would likely over-anneal to ensure malleability and ductility during further mechanical working and finishing.

Werner (1965) stated that larger grain sizes are a primary cause of silver embrittlement. This is incorrect – or at least imprecise – since large grain size silver is usually ductile (Wanhill *et al*. 1998), as attested also by the successful manufacture of archaeological silver artifacts, and by experiments on silver single crystals (Andrade and Henderson 1951; Rosi 1954). However, Werner's observations show that grain size must be an important, albeit secondary, factor for silver embrittlement.

The influence of grain size on microstructurally-induced embrittlement of archaeological silver may be explained as follows. Figure 12 shows a generic model of grain boundary microcrack initiation by a pile-up of crystal lattice dislocations on a crystal slip plane. The model's controlling parameters are the pile-up length, equal to the grain diameter d, and the grain

boundary fracture energy γ_f. Fracture mechanics provides the following condition for microcrack initiation (Smith and Barnby 1967):

$$\tau \geq \frac{3}{2}\sqrt{\frac{\pi \mu \gamma_f}{d}} \qquad (1)$$

where τ is the effective shear stress on the slip plane; π is the well-known transcendental number, approximately 3.142; and μ is the shear modulus of the crystal lattice for the crystal slip plane.

Equation (1) makes the general prediction that grain boundary microcrack initiation is easier when the grain diameter d is larger and the grain boundary fracture energy γ_f is smaller. In the context of microstructurally-induced embrittlement of archaeological silver, and given that a load or force is responsible for the effective shear stresses on slip planes, equation (1) implies that:

(3) Larger grain sizes permit longer dislocation pile-ups on slip planes and hence easier microcrack initiation along embrittled grain boundaries.

(4) Microcrack initiation along grain boundaries is easier (*in fact, made possible*) when the grain boundary fracture energy is reduced by impurity element segregation. This is directly linked to grain size also. Larger grains mean there is less boundary area to embrittle by a given amount of impurities, leading to increased concentrations of impurities at grain boundaries and increased embrittlement (Thompson and Knott 1993).

Both implications (3) and (4) are consistent with Werner's observations of a detrimental effect of larger grain size on the embrittlement of archaeological silver (Werner 1965). Furthermore, implication (4) enables a more specific formulation of implication (1), namely: *if* embrittling impurity elements have segregated to grain boundaries in archaeological silver, then the microstructure will be capable of providing many microcrack initiation sites and easy fracture paths for microcracks to become macrocracks. In other words, a microstructurally embrittled artifact is likely to be frangible, especially if it contains large grains.

DIAGNOSTIC TECHNIQUES FOR ARCHAEOLOGICAL SILVER EMBRITTLEMENT

Introduction: microstructurally-induced and corrosion-induced embrittlement

This report is concerned primarily with microstructurally-induced embrittlement of archaeological silver. But from a practical viewpoint we have to consider corrosion-induced embrittlement as well, especially since it may well be the predominant type of embrittlement.

Corrosion-induced embrittlement of archaeological silver is described and discussed in Appendix C, including its synergistic action with microstructurally-induced embrittlement.

Survey of diagnostic techniques

Table 3 surveys the diagnostic techniques for determining embrittlement of archaeological silver. The survey is based on Wanhill (2000a), Wanhill *et al*. (1998), and the previous sections of this report. Metallography is generally the most important diagnostic technique, especially when combined with chemical analysis by using SEM+EDX or SEM+WDX combinations: EDX is more widely available than WDX, which, however, is more accurate and better able to determine small amounts of impurity elements. Metallography is also an integral part of microhardness testing. For example, the lower metallograph in figure C.1 (Appendix C) shows a diamond-shaped microhardness indentation, whose size and hence HV value was measured with a specially-adapted optical microscope.

With respect to chemical composition, fully quantitative EDX or WDX analyses using elemental standards should provide two kinds of information. Firstly, the analyses should distinguish whether the silver was obtained from lead cupellation, native silver or aurian silver. (However, determination of provenance is more difficult: see, for example, Gale and Stos-Gale (1981).) Secondly, the lead, bismuth, antimony, tin, arsenic, thallium and copper contents are potentially important for diagnosing the types of silver embrittlement, as follows:

(1) Lead is most probably the key to microstructurally-induced embrittlement of silver. Long-term segregation or precipitation of lead at grain boundaries can occur at bulk contents less than 0.1 wt. %, see figure 1. Other impurity elements might be involved, becoming less likely in the order bismuth, arsenic, thallium, antimony and tin.

(2) Corrosion-induced embrittlement is partly or mainly due to copper segregation, see Appendix C. At low temperatures copper can segregate to grain boundaries, resulting in

cellular (or discontinuous) precipitation and intergranular corrosion. At high temperature copper segregates during alloy solidification. This type of segregation results in ambient temperature corrosion that is either interdendritic, in essentially as-solidified microstructures, or along copper-rich segregation bands. These bands are the remains of solute element segregation (coring) and interdendritic segregation that have been modified and reduced by mechanical working and annealing heat-treatments.

At present it is uncertain what the lowest bulk content of copper is that could enable long-term cellular precipitation and corrosion-induced intergranular embrittlement. The lower limit is probably between 1-3 wt. % copper (Schweizer and Meyers 1978; Wanhill *et al*. 1998). However, corrosion induced by high temperature copper segregation and possible long-term low temperature copper segregation along slip bands and deformation twin boundaries could cause embrittlement at even lower copper contents: the Egyptian silver vase investigated by Wanhill *et al*. (1998) contained only 0.9 wt. % copper.

NOTES

A Here it is appropriate to put the problem of archaeological silver embrittlement into perspective. The well-known researcher, Peter Northover, has studied some 300 silver vessels and analysed over 2000 silver alloy coins. Only a small proportion was badly embrittled (Northover 1999).

B Another important point is the primary significance of the lead and copper contents. Archaeological silver often contains more than 0.1 wt. % lead and more than 1-3 wt. % copper (Gale and Stos-Gale 1981a; Bennett 1994); see figure 11 and Appendix B also. Thus microstructurally-induced embrittlement owing to segregation or precipitation of lead and corrosion-induced embrittlement owing to cellular precipitation of copper should be due to an adverse combination of factors besides the lead and copper contents. These factors include the object's manufactured condition and burial time; and the average temperature and moisture content of the burial environment and its chemical composition, especially the salt, nitrate and nitrite contents (Gowland 1918).

C With respect to an object's manufactured condition, the retention of plastic deformation (cold-work) in the microstructure should facilitate and accelerate microstructurally-induced embrittlement by lead (Thompson and Chatterjee 1954) and cellular precipitation of copper (Hornbogen 1972; Pawlowski 1979a, 1979b). However, whether the latter leads to enhanced corrosion-induced embrittlement is questionable: Northover (1999) observes that "intergranular cracking/corrosion is most prevalent at low concentrations of copper,

i.e. in circumstances where discontinuous precipitation of copper is likely to be minimal, if present at all."

REMEDIAL MEASURES FOR ARCHAEOLOGICAL SILVER EMBRITTLEMENT

Modern restorations and conservation are concerned – or should be concerned – with both technical and ethical considerations. In principle, any treatments should be reversible. If not, they must be well justified from an art-historical viewpoint. Bearing these points in mind, table 4 illustrates how the basic condition and type of embrittlement of archaeological silver result in technically possible and potentially sanctionable remedies.

For example, nominally intact objects almost certainly would not be heat-treated, though coins are possible exceptions, as indicated in the right-hand column of table 4. On the other hand, if it is decided to restore severely embrittled and fragmented objects, then heat-treatment may be essential (Ravich 1993). The main objection to heat-treatments is that they change the microstructure, and therefore information about an object's manufactured condition and subsequent history can be partially or completely lost. Also important is that heat-treatments entail a risk of further damage. These considerations suggest most strongly that heat-treatments should be allowed only if preceded by thorough diagnostic investigations, e.g. see table 3, and if judged feasible and done by experienced technical staff.

Table 4 also includes a more acceptable remedial measure that is applicable to any embrittled object. This remedy is cleaning, outgassing to dry crack surfaces and any entrapped corrosion products, and application of a protective coating, all to stop further corrosion and embrittlement (Wanhill *et al*. 1998). Some conservators may regard a protective coating, usually to prevent tarnishing, as undesirable (Born 1986). However, even though corrosion-induced and synergistic embrittlement must be very slow processes, they will most probably continue if atmospheric moisture still has access to the cracks and corrosion damage. Thus in this context a protective coating is truly needed after cleaning and drying. The choice and application of any protective coating requires much care (van Reekum and Moll 2000)[*]. For cracked and corroded objects a "Parylene" coating may be the best option, see Wood (2000).

[*] April 1998 saw the start of a 3-year research project, Silprot, aimed at reducing the effects of air pollution on silver collections. This project is subsidised by the European Commission and is a joint effort by the Instituut Collectie Nederland and the Rijksmuseum in Amsterdam, Oxford Brooks University and the University of Glasgow.

The need to remove and exclude moisture is also why it may be sanctionable to disassemble old restorations and reassemble with modern non-hygroscopic adhesives and fillers, followed by outgassing and a protective coating. In fact, this is a good procedure, if feasible, whether or not the silver is embrittled by corrosion, since it ensures that not only cracks and entrapped corrosion products are dried, but also any externally-connected crevices between the metal and adhesives and fillers.

Finally, it has to be emphasized that although table 4 is quite detailed, it is no more than a guide for dealing with embrittled archaeological silver. Each case must be considered on its own merits.

CONCLUSIONS

(1) Microstructurally-induced embrittlement of archaeological silver is characterized by grain boundary fracture. The cracks are narrow and sharp, except where grains have become bodily displaced, and there is no evidence of plastic deformation of the grain boundaries.

(2) This type of embrittlement is most probably a consequence of long-term low temperature ageing, whereby segregation of an impurity element, or elements, occurs to grain boundaries. The candidate embrittling impurities are lead, bismuth, arsenic, thallium, antimony and tin, in that order. Lead is the most likely perpetrator, but this has yet to be established directly for archaeological silver.

(3) Archaeological silver artifacts probably contain many grain boundaries very susceptible to impurity element segregation and microstructurally-induced embrittlement, *if it has occurred*. This supposition combines with a generic model of grain boundary microcrack initiation to show that an embrittled artifact is likely to be frangible, especially if it contains large grains.

(4) Present knowledge enables identifying and explaining microstructurally-induced and corrosion-induced embrittlement of archaeological silver and specifying diagnostic techniques for determining them. However, remedial measures to be taken during restoration and conservation are less certain. Suggested remedies are intended to be used as a guide.

REFERENCES

Andrade, E.N. da C., and Henderson, C., 1951, The mechanical behaviour of single crystals of certain face-centered cubic metals, Philosophical Transactions of the Royal Society, A244, 177-203.

Bailey, A.R., 1961, A Text-Book of Metallurgy, Second Edition, MacMillan and Company Ltd, London, U.K.

Baluffi, R.W. (ed.), 1980, Grain Boundary Structure and Kinetics, American Society for Metals (ASM), Metals Park, Ohio, U.S.A.

Baker, H., and Okamoto H. (eds.), 1992, ASM Handbook, Volume 3, Alloy Phase Diagrams, Section 2, ASM International, Materials Park, Ohio, U.S.A.

Bennett, A., 1994, Technical examination and conservation, Chapter 2 in The Sevso Treasure Part One, Journal of Roman Archaeology, Supplementary Series Number Twelve.

Born, H., 1986, Material und Herstellungstechnik der Silberschale des Merenptah, Jahrbuch Preussischer Kulturbesitz, 23, 143-153.

Caley, E.R., 1964, Analysis of Ancient Metals, 36-79, Pergamon Press, Oxford, U.K.

Chadwick, G.A., and Smith, D.A. (eds.), 1976, Grain Boundary Structure and Properties, Academic Press, London, U.K.

Cope, L.H., 1972, The metallurgical analysis of Roman Imperial silver and *aes* coinage, Methods of Chemical and Metallurgical Investigation of Ancient Coinage (Editors E.T. Hall and D.M. Metcalf), 3-47, Royal Numismatic Society, London, U.K.

Cottrell, A.H., 1988, Introduction to the Modern Theory of Metals, 124-126, The Institute of Metals, London, U.K.

Darken, L.S., and Gurry, R.W., 1953, Physical Chemistry of Metals, 79-90, McGraw-Hill Book Company, New York, New York, U.S.A.

Ercker, L., 1574, Beschreibung allerfürnemisten mineralischen Ertzt und Berckwerksarten: see translation of Second Edition of 1580 by A.G. Sisco and C.S. Smith, 1951, Lazarus Ercker's

Treatise on Ores and Assaying, 80-81, 191-198, University of Chicago Press, Chicago, Illinois, U.S.A.

Gale, N.H., and Stos-Gale, Z.A., 1981a, Ancient Egyptian silver, Journal of Egyptian Archaeology, 67, 103-115.

Gale, N.H., and Stos-Gale, Z.A., 1981b, Lead and silver in the ancient Aegean, Scientific American, 244, 142-152.

Gleiter, H., 1996, Chapter 9 in Physical Metallurgy, Fourth Edition, Volume I (Editors R.W. Cahn and P. Haasen), Elsevier Science B.V., Amsterdam, The Netherlands.

Gordus, A.A., 1972, Neutron activation analysis of coins and coin-streaks, Methods of Chemical and Metallurgical Investigation of Ancient Coinage (Editors E.T. Hall and D.M. Metcalf), 127-148, Royal Numismatic Society, London, U.K.

Gordy, W, and Thomas, W.J.O., 1956, Electronegativities of the elements, Journal of Chemical Physics, 24, 439-444.

Gowland, W., 1918, Silver in Roman and earlier times: I. Pre-historic and proto-historic times, Archaeologia, 69, 121-160.

Gschneider, K.A., Jr., 1980, L.S. (Larry) Darken's contributions to the theory of alloy formation and where we are today, Theory of Alloy Phase Formation (Editor L.H. Bennett), 1-34, The Metallurgical Society of AIME, Warrendale, Pennsylvania, U.S.A.

Gust, W., Predel, B., and Diekstall, K., 1978, Zur diskontinuierlichen Ausscheidung in Silber -6,2 At. % - Kupfer-Dreikristallen, Zeitschrift für Metallkunde, 69, 75-80.

Hertzberg, R.W., 1983, Deformation and Fracture Mechanics of Engineering Materials, Second Edition, John Wiley and Sons, New York, U.S.A.

Hondros, E.D., and Seah, M.P., 1977, Segregation to interfaces, International Metallurgical Reviews, 22, 262-301.

Hornbogen, E., 1972, Systematics of the cellular precipitation reactions, Metallurgical Transactions, 3, 2717-2727.

Hultgren, R., Desai, P.D., Hawkins, D.T., Gleiser, M., Kelley, K.K., and Wagman, D.D., 1973, Selected Values of the Thermodynamic Properties of the Elements, American Society for Metals (ASM), Metals Park, Ohio, U.S.A.

Hume-Rothery, W., and Raynor, G.V., 1954, The Structure of Metals and Alloys, Third Edition, 100-108, 126-132, 194-210, The Institute of Metals, London, U.K.

Jones, H., 1937, The phase boundaries in binary alloys, part 2: the theory of the α, β phase boundaries, Proceedings of the Physical Society of London, 49, 250-257.

King, H.W., 1965, Structure of the pure metals, Chapter 2 in Physical Metallurgy (Editor R.W. Cahn), North-Holland Publishing Company, Amsterdam, The Netherlands.

La Niece, S., 1983, Niello: an historical and technical survey, Antiquaries Journal, 63, 279-297.

Lawn, B.R., 1993, Fracture of Brittle Solids, Second Edition, Cambridge University Press, Cambridge, U.K.

Lim, L.C., and Watanabe, T., 1990, Fracture toughness and brittle-ductile transition controlled by grain boundary character distribution (GBCD) in polycrystals, Acta Metallurgica et Materialia, 38, 2507-2516.

Lucas, A., 1928, Silver in ancient times, Journal of Egyptian Archaeology, 14, 313-319.

MacDowall, D.W., 1972, The Pre-Mohammedan coinage of Greater India: a preliminary list of some analyses, Methods of Chemical and Metallurgical Investigation of Ancient Coinage (Editors E.T. Hall and D.M. Metcalf), 371-381, Royal Numismatic Society, London, U.K.

Massalski, T.B. 1996, Chapter 3 in Physical Metallurgy, Fourth Edition, Volume I (Editors R.W. Cahn and P. Haasen), Elsevier Science B.V., Amsterdam, The Netherlands.

Massalski, T.B., Murray, J.L., Bennett, L.H., Baker, H., and Kacprzak, L. (eds.), 1986, Binary Alloy Phase Diagrams, Volume 1, 35, 43, 44, 59, 60, 303-305, American Society for Metals (ASM), Metals Park, Ohio, U.S.A.

McKerrell, H., and Stevenson, R.B.K., 1972, Some analyses of Anglo-Saxon and associated Oriental silver coinage, Methods of Chemical and Metallurgical Investigation of Ancient Coinage (Editors E.T. Hall and D.M. Metcalf), 195-209, Royal Numismatic Society, London, U.K.

McLean, D., 1957, Grain Boundaries in Metals, Oxford University Press, London, U.K.

Metcalf, D.M., 1972, Analyses of the metal contents of Medieval coins, Methods of Chemical and Metallurgical Investigation of Ancient Coinage (Editors E.T. Hall and D.M. Metcalf), 383-434, Royal Numismatic Society, London, U.K.

Niemeyer, B., 1997, Early 20th-century restorations and modern conservation treatments on archaeological silver objects, Metal 95, Proceedings of the International Conference on Metals Conservation (Editors I.D. MacLeod, S.L. Pennec and L. Robbiola), 190-195, James & James (Science Publishers) Ltd, London, U.K.

Northover, J.P., 1999, Personal Communication, Department of Materials, Oxford University, Oxford, U.K.

Pauling, L., 1945, The Nature of the Chemical Bond, Second Edition, 58-75, Cornell University Press, Ithaca, New York, U.S.A.

Pauling, L., 1947, Atomic radii and interatomic distances in metals, Journal of the American Chemical Society, 69, 542-553.

Pawlowski, A., 1979a, Discontinuous precipitation in deformed FCC solid solution, Scripta METALLURGICA, 13, 785-790.

Pawlowski, A., 1979b, Changes of free energy in the process of discontinuous precipitation in deformed FCC solid solution, Scripta METALLURGICA, 13,791-794.

Perea, A., and Rovira, S., 1995, The gold from Arrabalde, Prehistoric Gold in Europe: Mines Metallurgy and Manufacture (Editors G. Morteani and J.P. Northover), 471-490, Kluwer Academic Publishers, Dordrecht, The Netherlands.

Pettifor, D.G., 1984, A chemical scale for crystal-structure maps, Solid State Communications, 51, 31-34.

Pettifor, D.G., 1988, Structure maps for pseudobinary and ternary phases, Materials Science and Technology, 4, 675-691.

Philip, G., and Rehren, T., 1996, Fourth millenium BC silver from Tell esh-Shuna, Jordan: archaeometallurgical investigation and some thoughts on ceramic skeuomorphs, Oxford Journal of Archaeology, 15, 129-150.

Proctor, R.P.M., 1994, Chapter 1.3 in Corrosion, Volume 1, Metal/Environment Reactions, Third Edition (Editors L.L. Shreir, R.A. Jarman and G.T. Burstein), Butterworth-Heinemann Ltd, Oxford, U.K.

Raub, Ch.J., 1995, The metallurgy of gold and silver in prehistoric times, Prehistoric Gold in Europe: Mines, Metallurgy and Manufacture (Editors G. Morteani and J.P. Northover), 243-259, Kluwer Academic Publishers, Dordrecht, The Netherlands.

Ravich, I.G., 1993, Annealing of brittle archaeological silver: microstructural and technological study, in 10th Triennial Meeting of the International Council of Museums Committee for Conservation, Preprints of the Seminar: August 22/27, 1993, II, 792-795, Washington, D.C., U.S.A.

Reekum, J. van, and Moll, E., 2000, Het lakken van zilverwerk: van gebruiksvoorwerp naar museumobject, Zeven IJzersterke Verhalen over Metalen (Editors H.A. Ankersmit and J.A. Mosk), 74-79, Instituut Collectie Nederland, Amsterdam, The Netherlands.

Roberts-Austen, W.C., 1888, On certain mechanical properties of metals considered in relation to the Periodic Law, Philosophical Transactions of the Royal Society of London, A179, 339-350.

Rosi, F.D., 1954, Stress-strain characteristics and slip-band formation in metal crystals: effect of crystal orientation, Journal of Metals, 6, 1009-1020.

Scharfenberger, W., Schmitt, G., and Borchers, H., 1972, Über die Kinetik der diskontinuierlichen Ausscheidung der Silberlegierung mit 7,5 Gew.-%Cu, Zeitschrift für Metallkunde, 63, 553-560.

Schweizer, F., and Meyers, P., 1978, Authenticity of ancient silver objects: a new approach, MASCA Journal, 1, 9-10.

Scott, D.A., 1996, Technical study of a ceremonial Sican tumi figurine, Archaeometry, 38, 305-311.

Seah, M.P., 1980a, Adsorption-induced interface decohesion, Acta Metallurgica, 28, 955-962.

Seah, M.P., 1980b, Chemistry of solid - solid interfaces – A review of its characterization, theory, and relevance to materials science, Journal of Vacuum Science and Technology, 17, 16-24.

Shewmon, P.G., 1998, Grain boundary cracking, Metallurgical and Materials Transactions A, 29A, 1535-1544.

Smith, E., and Barnby, J.T., 1967, Crack nucleation in crystalline solids, Metal Science Journal, 1, 56-64.

Smithells, C.J., 1967, Metals Reference Book, Volume 2, Fourth Edition, Butterworths, London, U.K.

Teatum, E.T., Gschneider, K.A., Jr., and Waber, J.T., 1968, Compilation of calculated data useful in predicting metallurgical behavior of the elements in binary alloy systems, Los Alamos Scientific Laboratory Report LA-4003, Clearing House for Federal Scientific and Technical Information, Springfield, Virginia, U.S.A.

Thompson, A.W., and Knott, J.F., 1993, Micromechanisms of brittle fracture, Metallurgical Transactions A, 24A, 523-534.

Thompson, F.C., and Chatterjee, A.K., 1954, The age-embrittlement of silver coins, Studies in Conservation, 1, 115-126.

Tylecote, R.F., 1986, The Prehistory of Metallurgy in the British Isles, 3-4, 54-61, The Institute of Metals, London, U.K.

Tylecote, R.F., 1987, The Early History of Metallurgy in Europe, 69-80, 138-140, 280-290, Longman Inc., New York, New York, U.S.A.

Tylecote, R.F., 1992, A History of Metallurgy, Second Edition, 71, The Institute of Materials, London, U.K.

Waber, J.T., Gschneider, K.A., Jr., Larson, A.C., and Prince, M.Y., 1963, Prediction of solid solubility in metallic alloys, Transactions of the Metallurgical Society of AIME, 227, 717-723.

Wanhill, R.J.H., 2000a, Brittle archaeological silver. Identification, restoration and conservation, Materialen, 16, 30-35: also NLR Technical Publication NLR TP 97647 L, National Aerospace Laboratory NLR, Amsterdam, The Netherlands.

Wanhill, R.J.H., 2000b, Microstructural embrittlement of gold and silver, NLR Technical Publication NLR-TP-2000-358, National Aerospace Laboratory NLR, Amsterdam, The Netherlands.

Wanhill, R.J.H., Steijaert, J.P.H.M., Leenheer, R., and Koens, J.F.W., 1998, Damage assessment and preservation of an Egyptian silver vase (300-200 BC), Archaeometry, 40, 123-137: also NLR Technical Publication NLR TP 95372 L, National Aerospace Laboratory NLR, Amsterdam, The Netherlands.

Watanabe, T., 1984, An approach to grain boundary design for strong and ductile polycrystals, Res Mechanica, 11, 47-84.

Watanabe, T., 1993, Grain boundary design and control for high temperature materials, Materials Science and Engineering, A166, 11-28.

Watanabe, T., 1994, The impact of grain boundary character distribution on fracture in polycrystals, Materials Science and Engineering, A176, 39-49.

Watanabe, T., Kitamura, S., and Karashima, S., 1980, Grain boundary hardening and segregation in alpha iron-tin alloy, Acta Metallurgica, 28, 455-463.

Watanabe, T., Fujii, H., Oikawa, H., and Arai, K.I., 1989, Grain boundaries in rapidly solidified and annealed Fe-6.5 mass % Si polycrystalline ribbons with high ductility, Acta Metallurgica, 37, 941-952.

Werner, A.E., 1965, Two problems in the conservation of antiquities: corroded lead and brittle silver, in Application of Science in Examination of Works of Art (Editor W.J. Young), 96-104, Boston Museum of Fine Arts, Boston, Massachusetts, U.S.A.

Wood, R., 2000, To protect and preserve, Materials World, 8, 30-32.

Table 1 Selected metallic and semi-metallic element properties

ELEMENT	ATOMIC NUMBER	EMPIRICAL ORDERING NUMBER	ATOMIC DIAMETER (nm)	PAULING ATOMIC DIAMETER, C.N.12 (nm)	ALLOYING ELEMENT PRIMARY SOLID SOLUBILITY LIMIT IN SILVER		ELECTRO-NEGATIVITY $(eV)^{1/2}$	NUMBER OF VALENCE ELECTRONS	SUBLIMATION ENTHALPY (J/m^2)
					wt.%	at.%			
Li	3	12	0.3456	0.3098	9.1	60.9	0.95	1	3.37
Na	11	11	0.4226	0.3792	0	0	0.95	1	1.53
Al	13	80	0.3164	0.2858	6.1	20.6	1.52	3	8.34
K	19	10	0.5236	0.4698	0	0	0.83	1	0.84
Mn	25	60	0.2856	0.2522;0.2612	31	47	2.24;1.92	7;5	8.83
Cu	29	72	0.2826	0.2552	8.8	14.1	1.82	1	10.7
Zn	30	76	0.3076	0.2758	29.0	40.3	1.66	2	3.50
Ga	31	81	0.3344	0.2816	12.0	17.4	1.80	3	6.19
Ge	32	84	0.3510	0.2732	6.7	9.6	1.90	4	7.70
As	33	89	0.3452	0.2780	5.5	7.7	2.08	5	6.46
Se	34	93	0.3726	0.280	0	0	2.46	6	3.79
Rb	37	9	0.5600	0.4960	0	0	0.83	1	0.67
Rh	45	65	0.2974	0.2684	0	0	2.20	9	15.9
Pd	46	69	0.3042	0.2746	100	100	2.21	10	10.4
Ag	47	71	0.3196	0.2884	100	100	1.68	1	7.09
Cd	48	75	0.3452	0.3086	43.2	42.2	1.58	2	2.40
In	49	79	0.3682	0.3320	22.1	21.1	1.82	3	4.58
Sn	50	83	0.3724	0.3084;0.3240	12.5	11.5	1.83;1.65	4;2	5.55
Sb	51	88	0.3864	0.3180	8.1	7.2	1.98	5	4.52
Te	52	92	0.4010	0.320	0	0	1.92	6	3.12
Au	79	70	0.3188	0.2878	100	100	1.90	1	9.25
Tl	81	78	0.3784	0.3424	13.8	7.8	1.86	3	3.24
Pb	82	82	0.3898	0.3492	5.2	2.8	1.93	4	3.29
Bi	83	87	0.4072	0.340	4.9	2.6	1.86	5	3.23

(1) Empirical ordering number acknowledges chemical similarity of elements from the same Group of the Periodic Table (Pettifor 1988).

(2) Atomic diameters from King (1965) and Pauling (1947). The latter depend on the number of nearest neighbour atoms (coordination number, C.N.) for each atom in solid solution in the matrix. C.N.=12 for atoms in solid solution in silver.

(3) Primary solid solubility limits from Baker *et al*. (1992) and Massalski *et al*. (1986).

(4) Electronegativities and number of valence electrons from Teatum *et al*. (1968).

(5) Sublimation enthalpies (per unit area) according to Seah (1980a) using Hultgren *et al*. (1973).

Table 2 Silver binary alloys with alloying element low primary solid solubility: PSSL = Primary Solid Solubility Limit; max = maximum; eut = eutectic temperature; amb = ambient temperatures. Data (phase diagrams) from Baker et al. (1992), see Appendix A, and Thompson and Chatterjee (1954)

2.1 Zero or very low PSSL

BINARY ALLOY SYSTEMS	DILUTE ALLOY PHASE DIAGRAM CHARACTERISTICS	EQUILIBRIUM PHASES AT AMBIENT TEMPERATURES	
		PRIMARY CRYSTALS/GRAINS	BETWEEN PRIMARY CRYSTALS/GRAINS
Ag-K	phase diagram not available (Massalski *et al.* 1986)	Ag	
Ag-Na	Ag-Ag_2Na peritectic, 322°C ?; Ag-Na eutectic, > 99.9 at.% Na, 97.7°C	Ag	Na or possibly Ag_2Na
Ag-Rb	phase diagram not available (Massalski *et al.* 1986)	Ag	
Ag-Se	monotectic, 890°C; Ag-Ag_2Se eutectic, 12.1 at.% Se, 840°C	Ag	eutectic Ag+Ag_2Se
Ag-Te	Ag-Ag_2Te eutectic, 11.5 at.% Te, 869°C	Ag	eutectic Ag+Ag_2Te

2.2 $PSSL_{max}$ at eutectic or peritectic temperatures

BINARY ALLOY SYSTEMS	DILUTE ALLOY PHASE DIAGRAM CHARACTERISTICS	ALLOYING ELEMENT		EQUILIBRIUM PHASES AT AMBIENT TEMPERATURES		
				PRIMARY CRYSTALS/GRAINS		BETWEEN PRIMARY CRYSTALS/GRAINS
		$PSSL_{max}$ (at.%)	$PSSL_{amb}$ (at.%)	ALLOYS BELOW $PSSL_{amb}$	ALLOYS ABOVE $PSSL_{amb}$	ALLOYS ABOVE $PSSL_{max}$
Ag-As	α-ζ peritectic (up to 10.1 at.% As), 582°C; eutectoid, 446°C	7.7	~2?	α	α→α+As	eutectoid α+As
Ag-Ge	α-Ge eutectic, 24.2 at.% Ge, 651°C	9.6	~0		α→Ag+Ge	Ag+Ge from eutectic α+Ge
Ag-Sb	α-ζ peritectic (up to 8.8 at.% Sb), 702.5°C	7.2	~4	α	α→α+ζ	ζ (intermediate phase)
Ag-Sn	α-ζ peritectic (up to 12.9 at.% Sn), 724°C	11.5	~9	α	α→α+ζ	ζ (intermediate phase)

2.3 $PSSL_{max}$ > $PSSL_{eut}$

BINARY ALLOY SYSTEMS	DILUTE ALLOY PHASE DIAGRAM CHARACTERISTICS	ALLOYING ELEMENT			EQUILIBRIUM PHASES AT AMBIENT TEMPERATURES		
					PRIMARY CRYSTALS/GRAINS		BETWEEN PRIMARY CRYSTALS/GRAINS
		$PSSL_{max}$ (at.%)	$PSSL_{eut}$ (at.%)	$PSSL_{amb}$ (at.%)	ALLOYS BELOW $PSSL_{amb}$	ALLOYS ABOVE $PSSL_{amb}$	ALLOYS ABOVE $PSSL_{eut}$
Ag-Bi	α-Bi eutectic, 95.3 at.% Bi, 262.5°C	2.6	0.83	~0		α→Ag+Bi	Ag+Bi from eutectic α+Bi
Ag-Pb	α-Pb eutectic, 95.5 at.% Pb, 304°C	2.8	0.79	<0.05	α	α→α+Pb	α+Pb from eutectic α+Pb
Ag-Tl	α-Tl eutectic, 97.4 at.% Tl, 291°C	7.8	5.1	?	α	α→α+Tl	α+Tl from eutectic α+Tl

Table 3 Diagnostic techniques for microstructurally-induced and corrosion-induced embrittlement of archaeological silver. Corrosion-induced embrittlement is described in Appendix C

VISUAL INSPECTION (×1-×10) (UNAIDED EYE AND HAND LENS)	X-RAY RADIOGRAPHY (×1) (LIMITED ENLARGEMENT)	OPTICAL (×10-×1000) AND SEM (×10-×30,000) METALLOGRAPHY, EDX OR WDX, AND MICROHARDNESS TESTING (HV)	SEM FRACTOGRAPHY (×10-×30,000)

Purpose: Artifact Basic Condition
 	
• nominally intact
 	
• restored
  • macrocrack patterns
  • missing pieces
 	
• fragmented
  • macrocrack patterns
  • missing pieces
	Purpose: "Hidden" Damage
	
	• nominally intact, restored, or fragmented
	  • hairline cracks
	  • macrocracks
	  • cracks following indented decorations
	
	• restored
	  • missing pieces
		Purpose: Manufactured Condition, Chemical Analysis, Internal Damage and Embrittlement
		
		• manufactured condition
		  • mechanically worked — grain size, segregation bands, slip lines
		  • mechanically worked and annealed — deformation and annealing twins
		  • as-cast (dendritic) — coring, eutectic distribution
		  • cast and annealed (cellular)
		
		• chemical analysis (SEM + EDX or WDX)
		  • source: lead cupellation, native silver or aurian silver
		  • lead , bismuth, antimony, tin, arsenic and thallium contents: linked to microstructurally-induced embrittlement
		  • copper content
		  - high purity (low copper) may be linked to retained cold-work
		  - intentional additions of copper for strength
		  - long-term cellular precipitation along grain boundaries
		
		• microstructurally-induced embrittlement
		  • narrow intergranular cracks
		  • bodily displaced grains
		
		• corrosion-induced embrittlement
		  • surficial
		  • wide intergranular cracks: linked to cellular precipitation of copper
		  • interdendritic
		  • corrosion along segregation bands, slip lines, deformation twin boundaries and in slip-line fields below indented decorations: severe corrosion leads to cracks
		
		• microhardness testing (HV)
		  • annealed — HV values also depend on chemistry, especially copper content
		  • retained cold-work
		  • microstructural embrittlement — HV values and possible nucleation of new cracks
		  • corrosion
			Purpose: Embrittlement Types
			
			• microstructural embrittlement
			  • mainly clean grain boundary facets: can show local corrosion where slip lines, deformation twins and segregation bands intersect the fracture surfaces
			  • narrow intergranular cracks
			  • bodily displaced grains
			
			• corrosion-induced embrittlement
			  • surficial corrosion
			  • corroded fracture surfaces with fine granular appearance like surficial corrosion
			  • transgranular fracture (crystallographic) along slip bands and deformation twin boundaries, possibly also along annealing twin boundaries

SEM = Scanning Electron Microscopy; EDX = Energy Dispersive X-ray fluorescence; WDX = Wavelength Dispersive X-ray fluorescence

Table 4 Possible remedial measures for embrittled archaeological silver

ARTIFACT BASIC CONDITION		TYPE OF EMBRITTLEMENT	TECHNICALLY POSSIBLE REMEDIES	POTENTIALLY SANCTIONABLE REMEDIES
Nominally Intact	undeformed	• microstructurally-induced • corrosion-induced; synergistic	• A • B	• none • B
	deformed	• microstructurally-induced • corrosion-induced; synergistic	• A • B • C	• A : coins • B • C : coins
Restored	old restoration	• microstructurally-induced • corrosion-induced • synergistic	• disassembly + A + reassembly • B • disassembly + reassembly + B • disassembly + C + reassembly • B	• none • B • disassembly + reassembly + B • B
	modern restoration	• microstructurally-induced • corrosion-induced; synergistic	• disassembly + A + reassembly • B	• none • B
Fragmented		• microstructurally-induced • corrosion-induced; synergistic	• A + assembly • C + assembly • assembly + B	• A + assembly • C + assembly • assembly + B

NOTES

A Heat in an inert environment (e.g. argon or nitrogen) for 0.5-1 hour at 500 °C, cool in a forced air draught. This is based on data and suggestions of Thompson and Chatterjee (1954) for silver containing copper as well as lead. The heat-treatment's efficacy may be checked by microhardness testing (no new cracks).

B Restore original surface finish, if necessary. Clean and rinse successively in demineralised water and ethanol. Outgas *in vacuo* ($<10^{-4}$ Pa) and place in desiccator to await coating. Apply a colourless transparent organic coating, e.g. an acrylic resin, aliphatic polyurethane or cellulose nitrate "Frigilene"(Wanhill *et al.* 1998; van Reekum and Moll 2000). Probably the best option would be a "Parylene"coating, deposited by vapour condensation under a reduced pressure of 15 Pa (Wood 2000).

C Heat in an inert environment or under charcoal for 5-10 minutes at 700 °C, cool in a forced air draught. This is based on Ravich (1993). Prior heating in flowing hydrogen for 0.5 hour at 300-400 °C could be beneficial (Werner 1965), presumably because some of the intergranular corrosion products – notably silver chloride – are converted back to metal.
The heat-treatment temperature of 700 °C is probably close to the minimum, see Ravich (1993). Higher temperatures may have to be considered. This is very problematical, although successful experiments have been done at temperatures up to 900 °C (Werner 1965; Ravich 1993).

Coins : These are relatively small and therefore easier to heat-treat, even by hand.

Old restorations : Disassembly and reassembly may be feasible and required. Reassemble with modern non-hygroscopic adhesives and fillers (Niemeyer 1997).

Composite objects : A and C assume artifacts do not have soldered joints or niello inlay or gilding. Soft solders (lead-tin) begin melting above 183 °C (Bailey 1961, 513) and will also dissolve the silver if overheated (Niemeyer 1997). Hard solders (silver-copper) begin melting above 779 °C (Smithells 1967, 379). Roman silver sulphide niello should not be heated much above 600 °C, and later silver-copper and silver-copper-lead sulphide niellos melt at about 680 °C and 440 °C respectively (La Niece 1983, Bennett 1994). Gilding is easily ruined by (over)heating: gold layers are so thin, ~10 μm, they soon diffuse into the silver substrate.

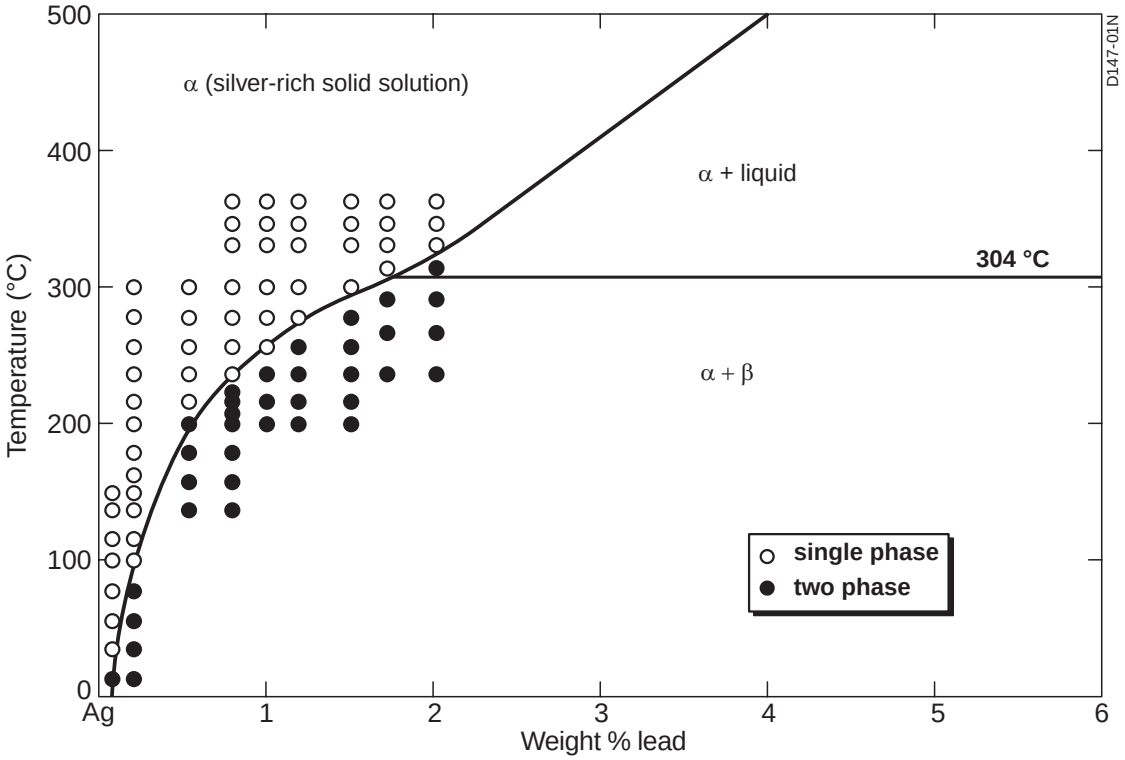

Fig. 1 Silver-rich low temperature region of the Ag-Pb equilibrium phase diagram, determined by ageing supersaturated solid solutions at the indicated temperatures (Thompson and Chatterjee 1954)

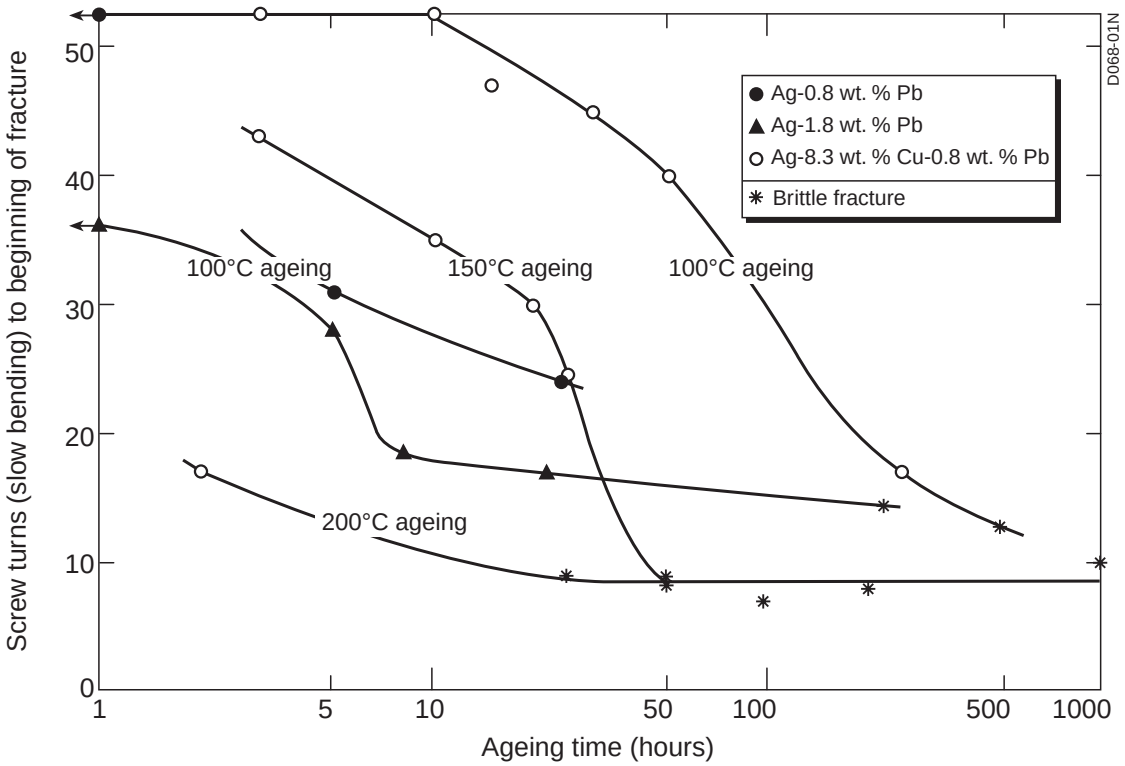

Fig. 2 Age-embrittlement of cast, solution treated and aged Ag-Pb and Ag-Cu-Pb alloys. Data from Thompson and Chatterjee (1954)

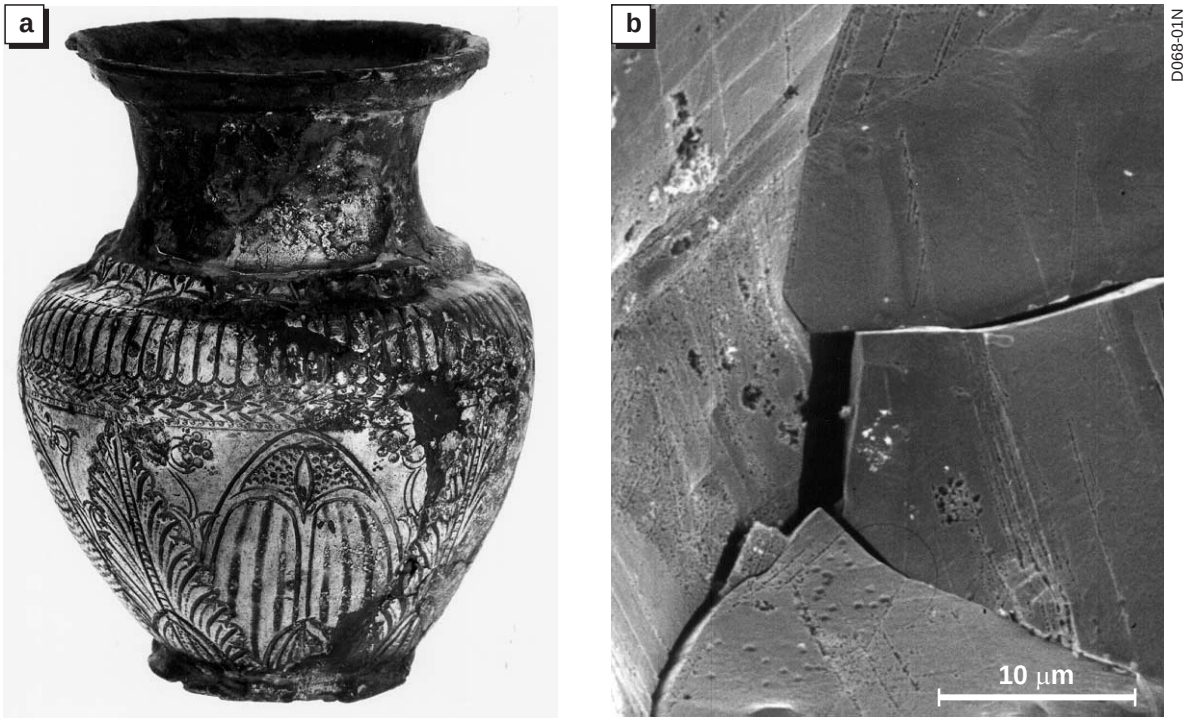

Fig. 3 Brittle grain boundary fracture in a sample from an Egyptian silver vase (Wanhill et al.1998)

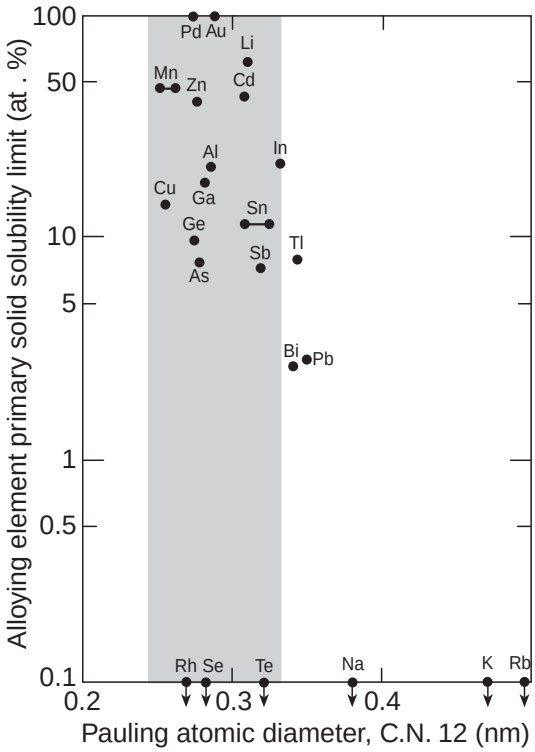

Fig. 4 The size-factor rule for solid solutions in silver. The shaded regions shows the range of favourable size-factor, bounded by the limits ±15% of the atomic diameter of silver. Data from table 1

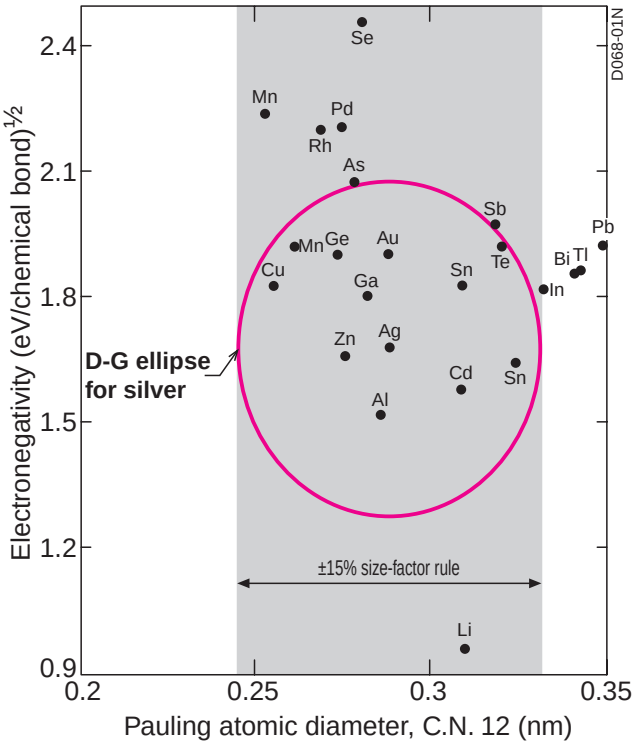

Fig. 5 Darken-Gurry (D-G) map for solid solutions in silver. Solute elements within the ellipse boundary, minor axes ±0.4 (eV)½, are predicted to have solid solubilities greater than 5-10 at . % . Data from table 1

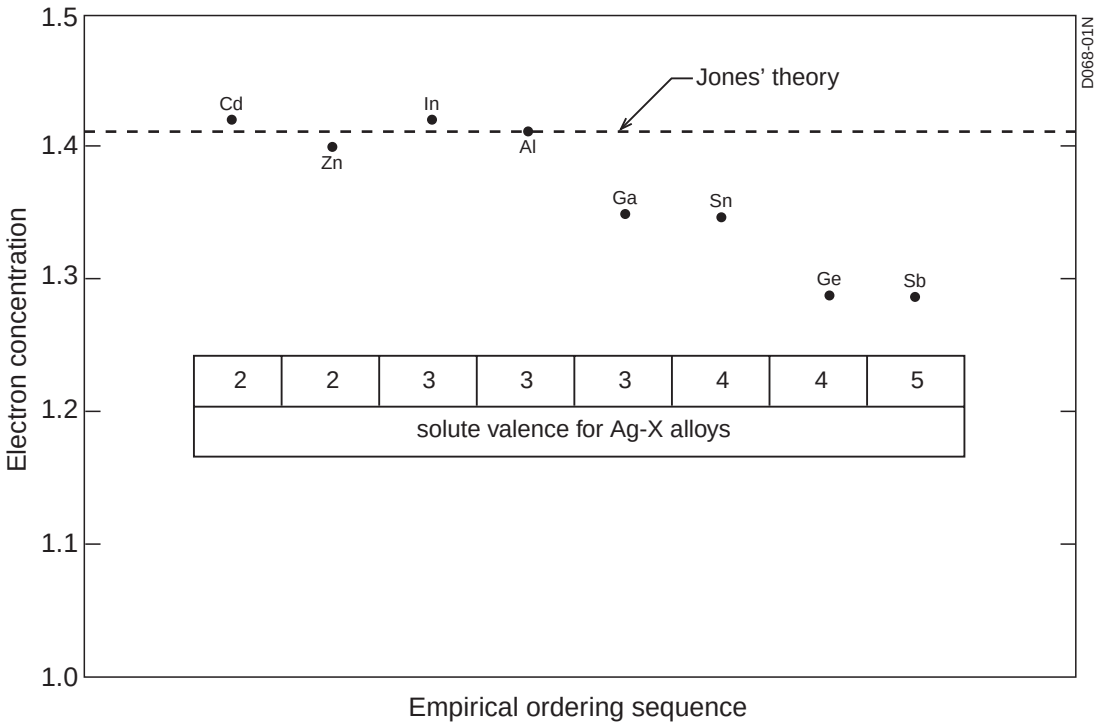

Fig. 6 B-subGroup alloying element primary solid solubility limits in silver, expressed as electron concentrations, [V(100-PSSL)+vPSSL]/100, where PSSL is the primary solid solubility limit in at. % and V and v are the number of valence electrons of the solvent and solute respectively. Data from table 1

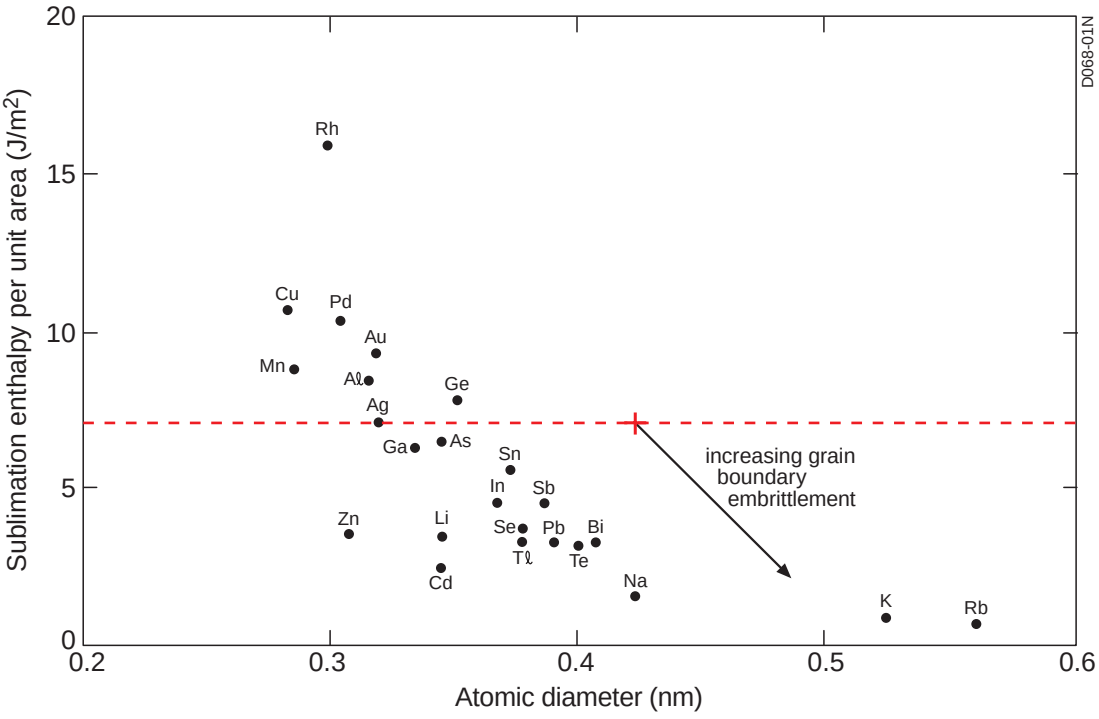

Fig. 7 Embrittlement plot for matrix (Ag) and segregant elements. After Seah (1980a), data from table 1

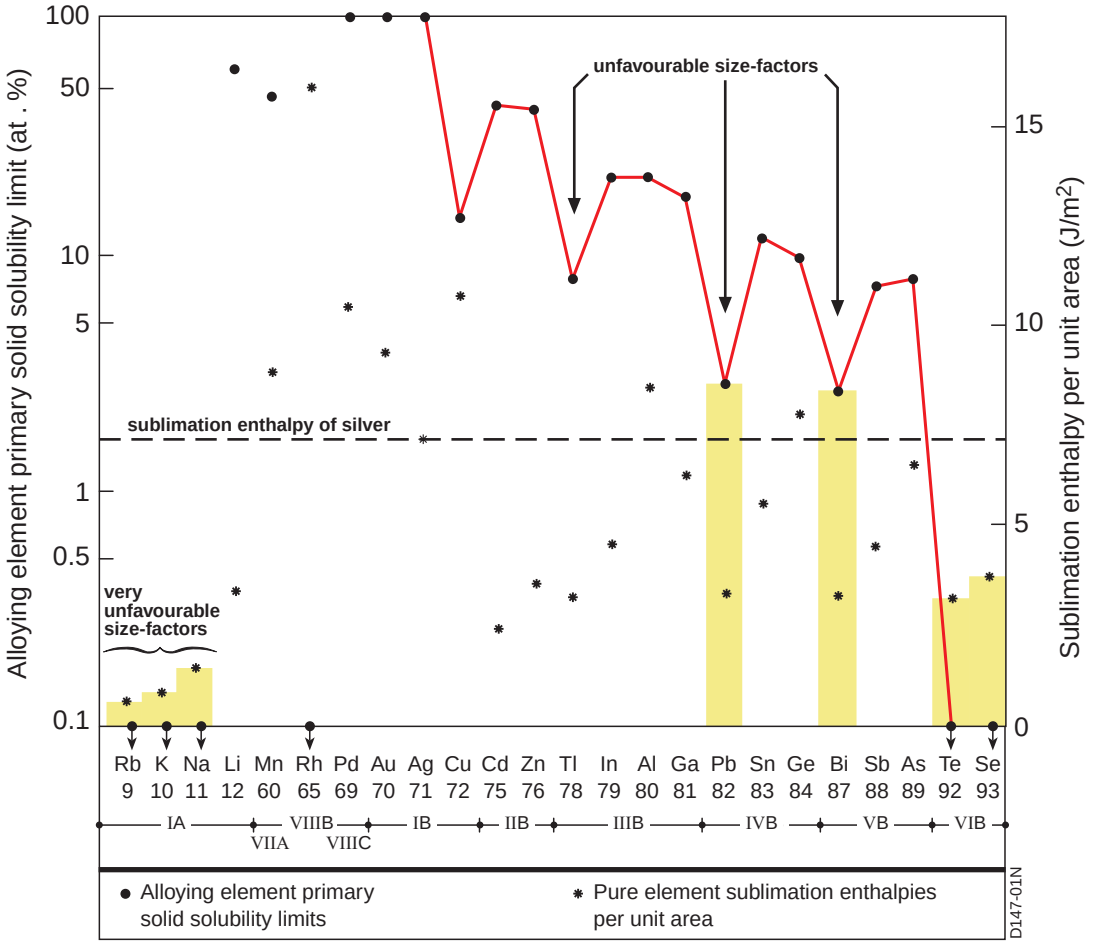

Fig. 8 Correlations between alloying element primary solid solubility limits in silver and the pure element sublimation enthalpies per unit area. The numerical sequence of the elements is the empirical ordering due to Pettifor (1988). The shaded regions denote the matrix and alloying element combinations that would seem most likely to result in segregation-induced grain boundary fracture under equilibrium conditions (see text). Data from table 1

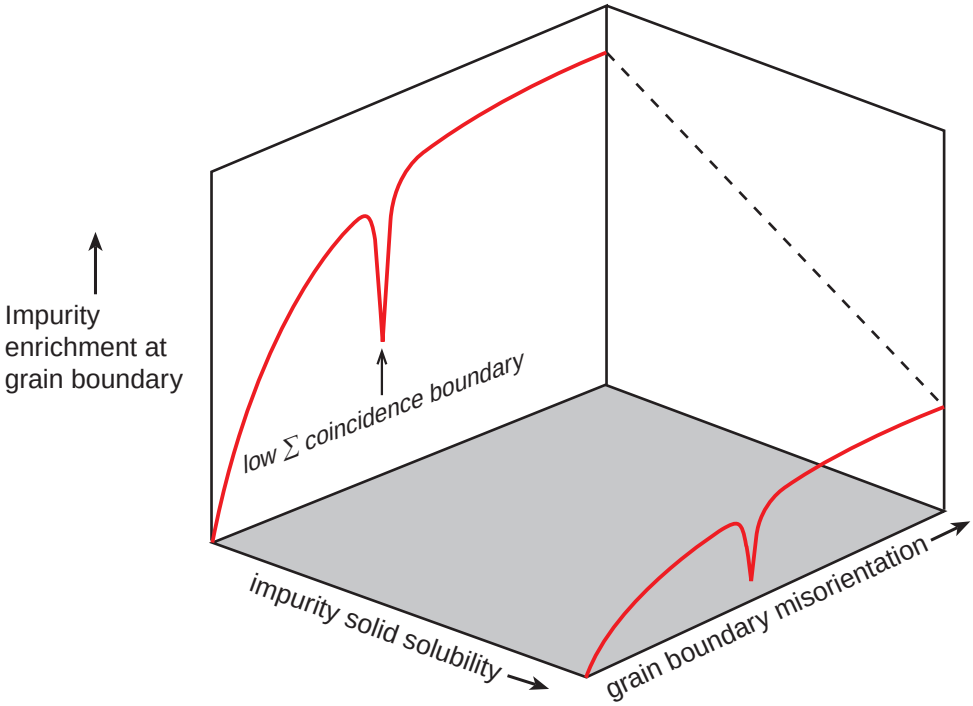

Fig. 9 *Schematic grain boundary segregation diagram for grain boundaries with misorientations about a specific axis of rotation. After Watanabe* et al. *(1980)*

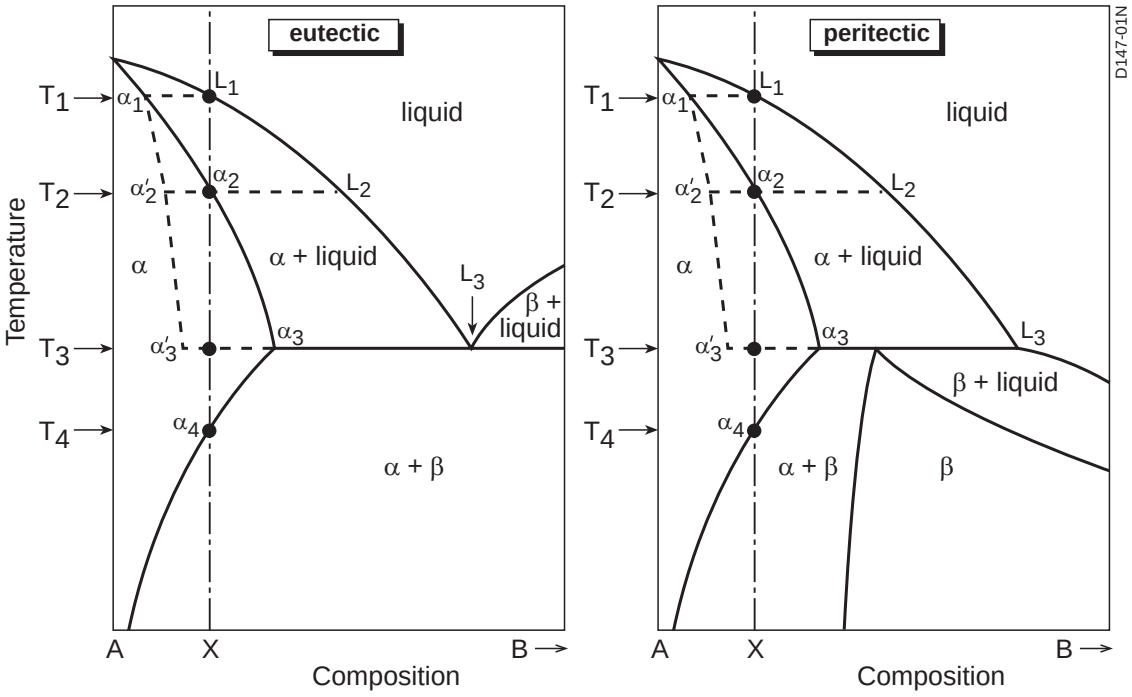

Fig. 10 *Schematic binary alloy equilibrium phase diagrams involving eutectic or peritectic reactions and illustrating the effect of non-equilibrium cooling on solidification of dilute alloys of bulk composition X (see text)*

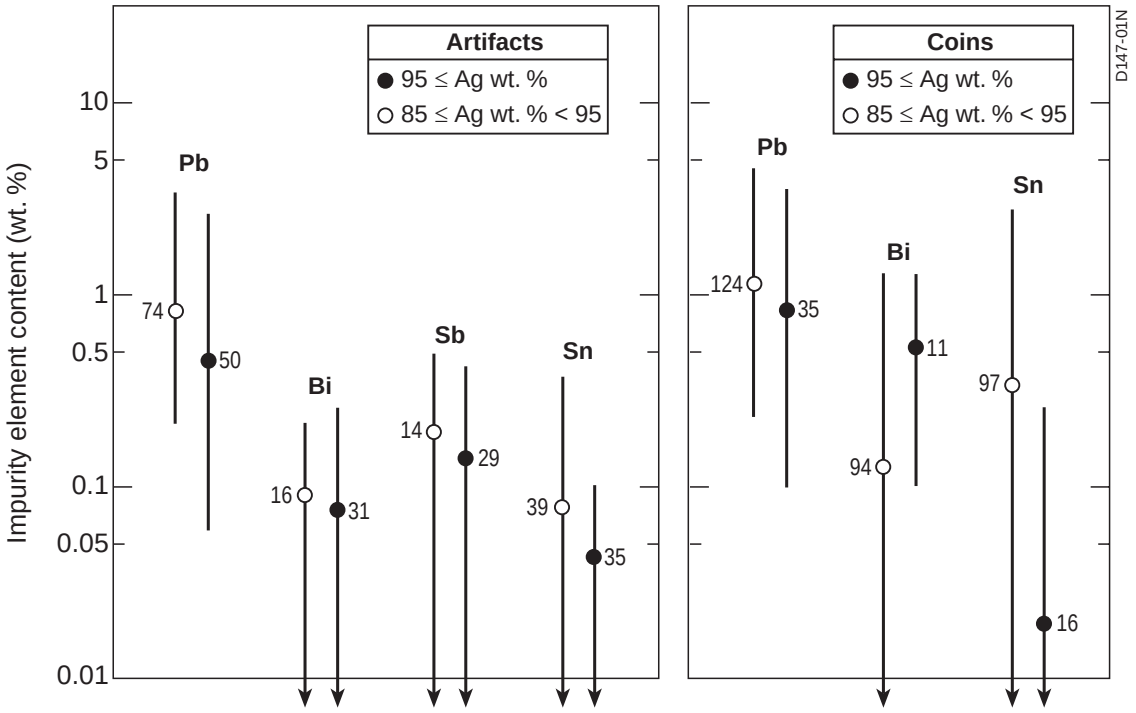

Fig. 11 Actually or potentially embrittling impurity elements in archaeological silver artifacts and coins. Data from Lucas (1928), Caley (1964), Cope (1972), Gordus (1972), MacDowall (1972), McKerrell and Stevenson (1972), Metcalf (1972), Gale and Stos-Gale (1981a), Tylecote (1992), Bennett (1994) and Perea and Rovira (1995), see Appendix B

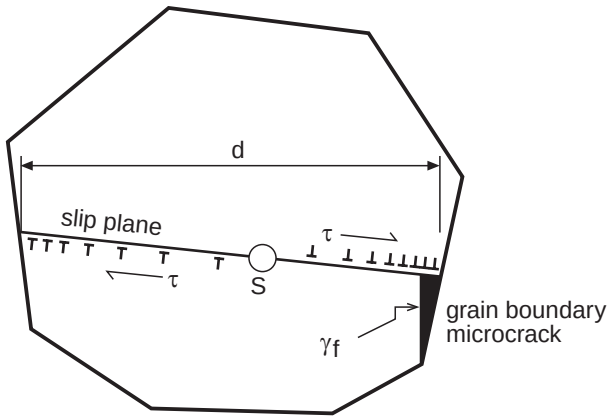

γ_f : grain boundary fracture energy
d : grain diameter/dislocation pile-up length
S : dislocation source
τ : effective shear stress on the slip plane
$\perp$: edge-type component of dislocation loop

Fig. 12 Generic model of initiation of a microcrack by dislocation pile-up. Under the effective shear stress τ the source S generates dislocation loops which pile-up at barriers (the grain boundaries) in the slip plane. The resulting stress concentrations initiate microcracks at one or both of the barriers. After Lawn (1993, 318) and Thompson and Knott (1993)

Appendix A Silver binary alloy equilibrium phase diagrams in support of table 2

A.1 Atomic weights

ELEMENT	SYMBOL	ATOMIC WEIGHT*	ELEMENT	SYMBOL	ATOMIC WEIGHT*
silver	Ag	107.880	antimony	Sb	121.76
arsenic	As	74.91	selenium	Se	78.96
bismuth	Bi	209.00	tin	Sn	118.70
germanium	Ge	72.60	tellurium	Te	127.61
sodium	Na	22.997	thallium	Tl	204.39
lead	Pb	207.21			

* As published in the Journal of the American Chemical Society, April 1950.

A.2 Interconversion of weight and atomic percentages in binary alloy systems

If w_x and a_x represent the weight and atomic percentages of one component having atomic weight x, and if w_y, a_y and y represent the corresponding quantities for the second component, then:

$$w_y = 100 - w_x$$
$$a_y = 100 - a_x$$

The conversion from weight to atomic percentages, or vice versa, may be made by use of the following formulae:

$$a_x = \frac{100}{1 + (x/y)[(100/w_x) - 1]}$$

$$w_x = \frac{100}{1 + (y/x)[(100/a_x) - 1]}$$

A.3 Phase diagrams (courtesy of ASM International)

A.3.1 Alloying elements with zero or very low primary solid solubilities

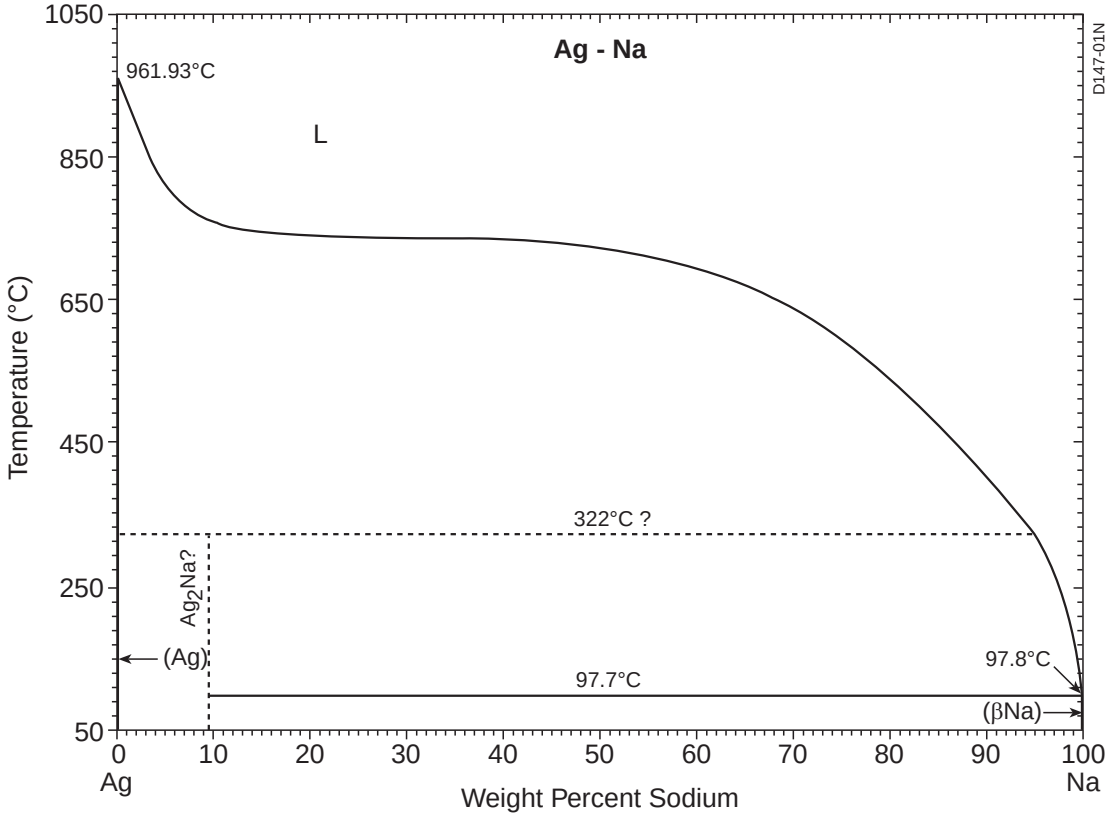

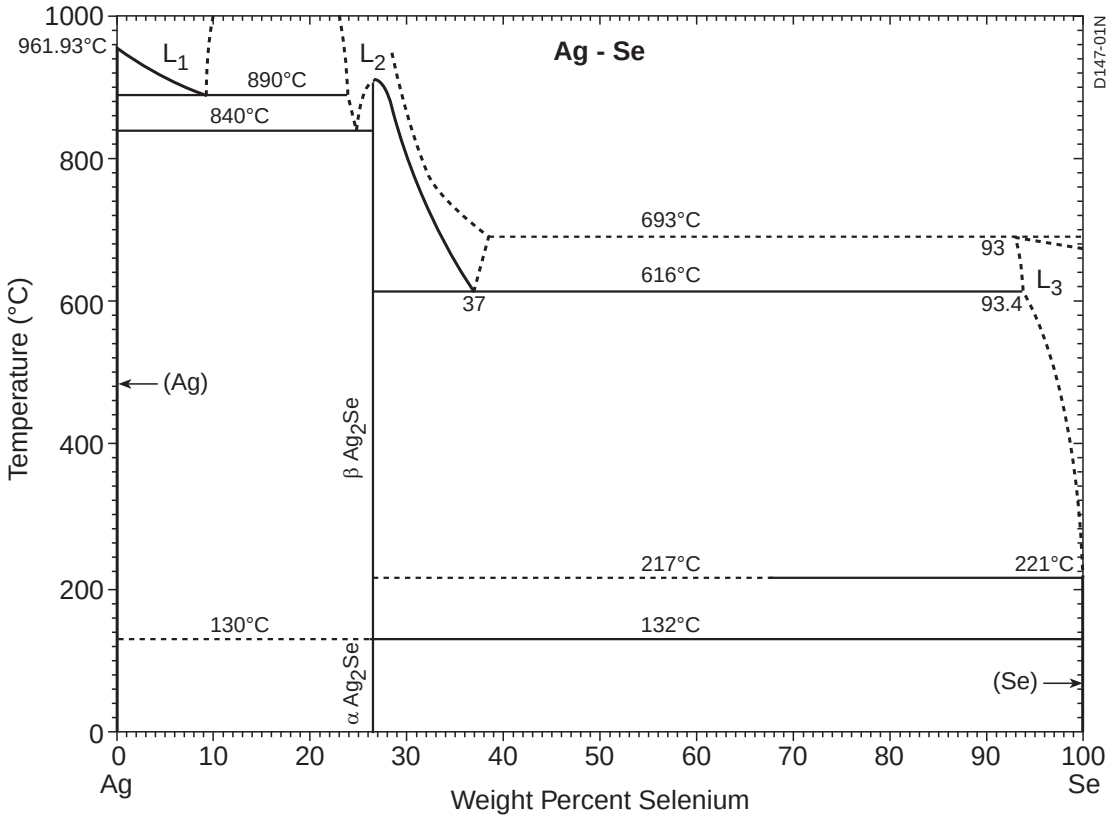

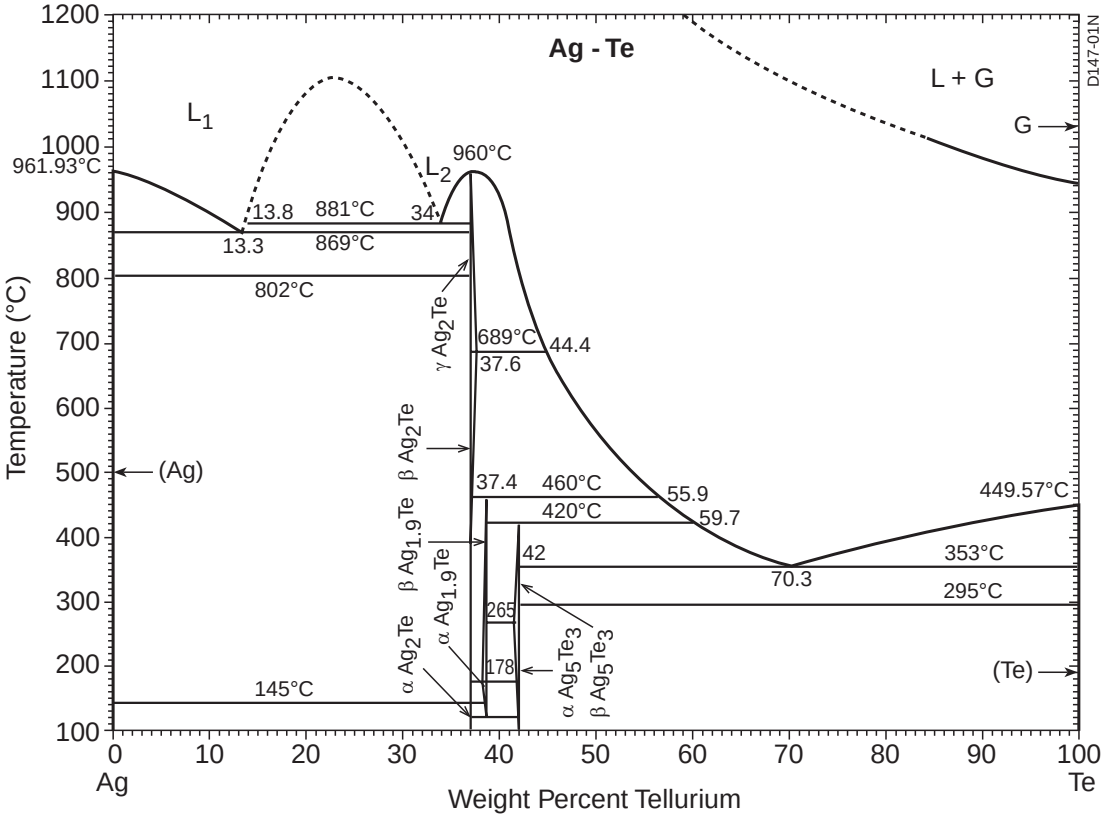
Ag - Te
D147-01N
L1
L2
L + G
G
960°C
961.93°C
13.8
881°C
34
13.3
869°C
802°C
γ Ag2Te
689°C
44.4
37.6
β Ag2Te
(Ag)
37.4
460°C
55.9
420°C
59.7
449.57°C
β Ag1.9Te
42
353°C
70.3
α Ag1.9Te
295°C
265
α Ag2Te
α Ag5Te3
β Ag5Te3
178
145°C
(Te)
Temperature (°C)
1200
1100
1000
900
800
700
600
500
400
300
200
100
0
10
20
30
40
50
60
70
80
90
100
Ag
Te
Weight Percent Tellurium

A.3.2 Alloying elements with maximum primary solid solubilities at eutectic or peritectic temperatures

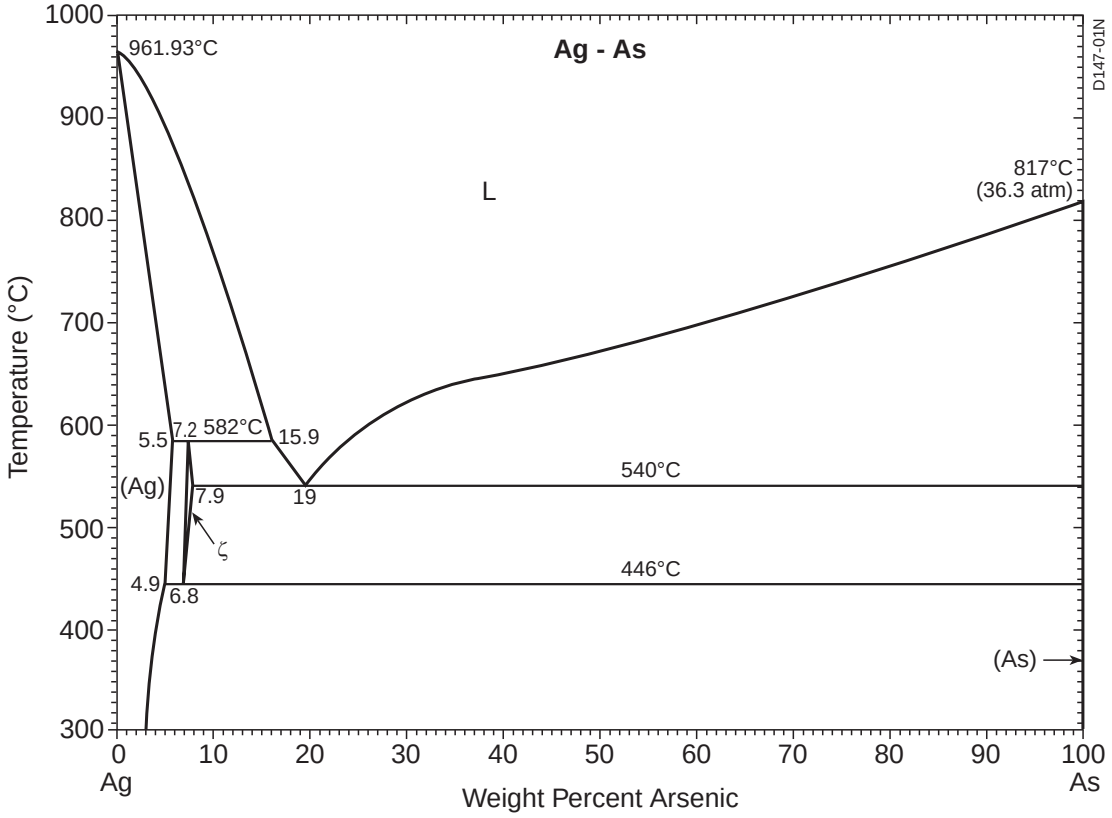

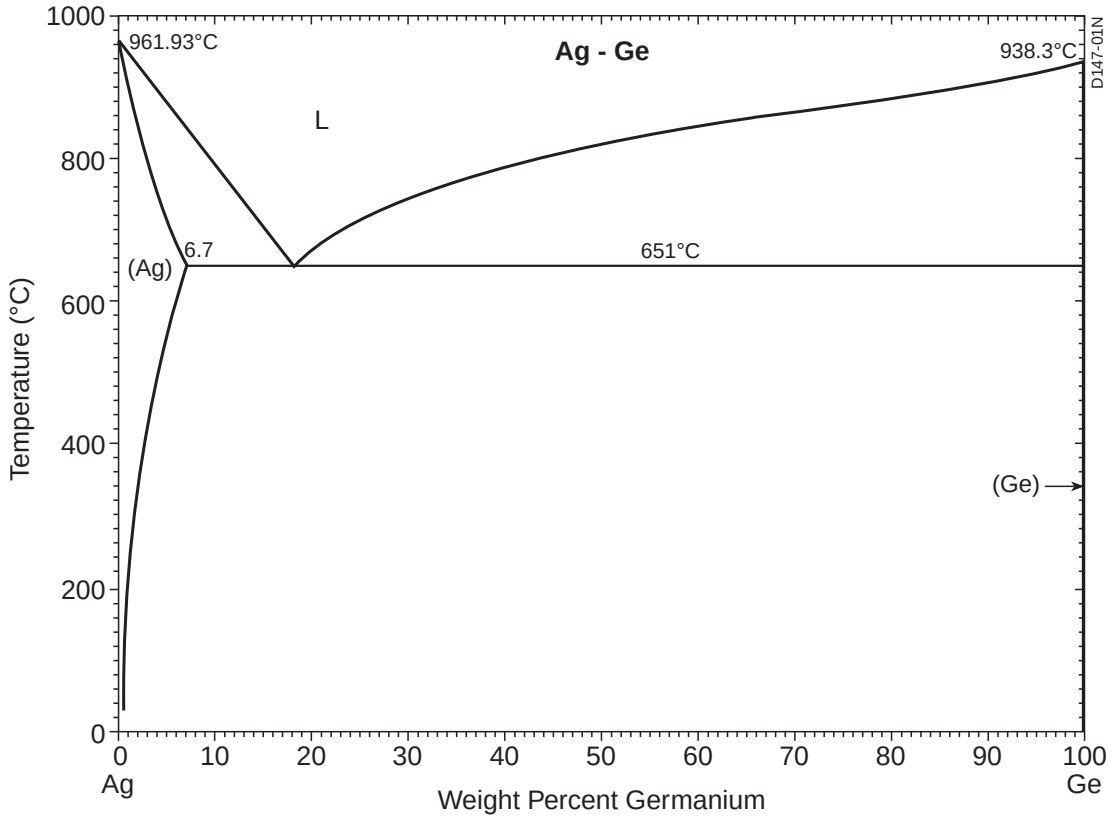

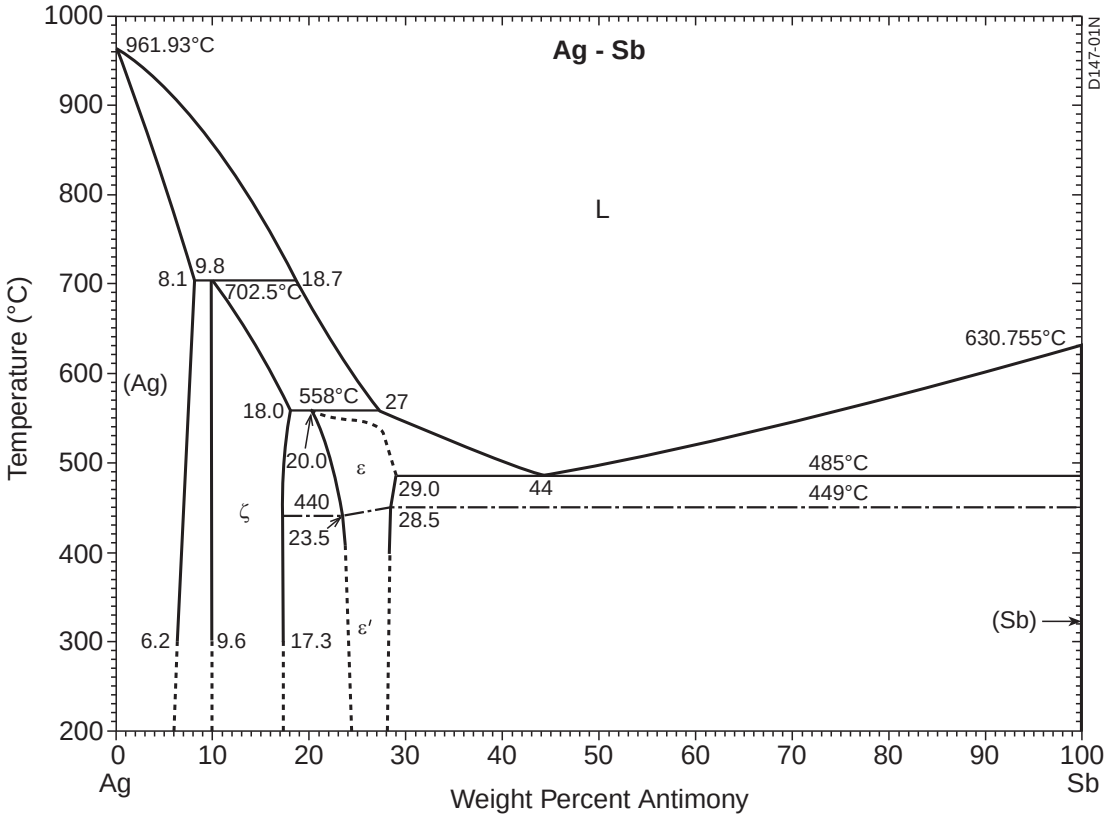
Ag - Sb
D147-01N
Temperature (°C)
Weight Percent Antimony
Ag
Sb
961.93°C
L
(Ag)
8.1
9.8
18.7
702.5°C
630.755°C
18.0
558°C
27
20.0
ε
485°C
29.0
44
449°C
440
28.5
23.5
ζ
ε′
(Sb)
6.2
9.6
17.3

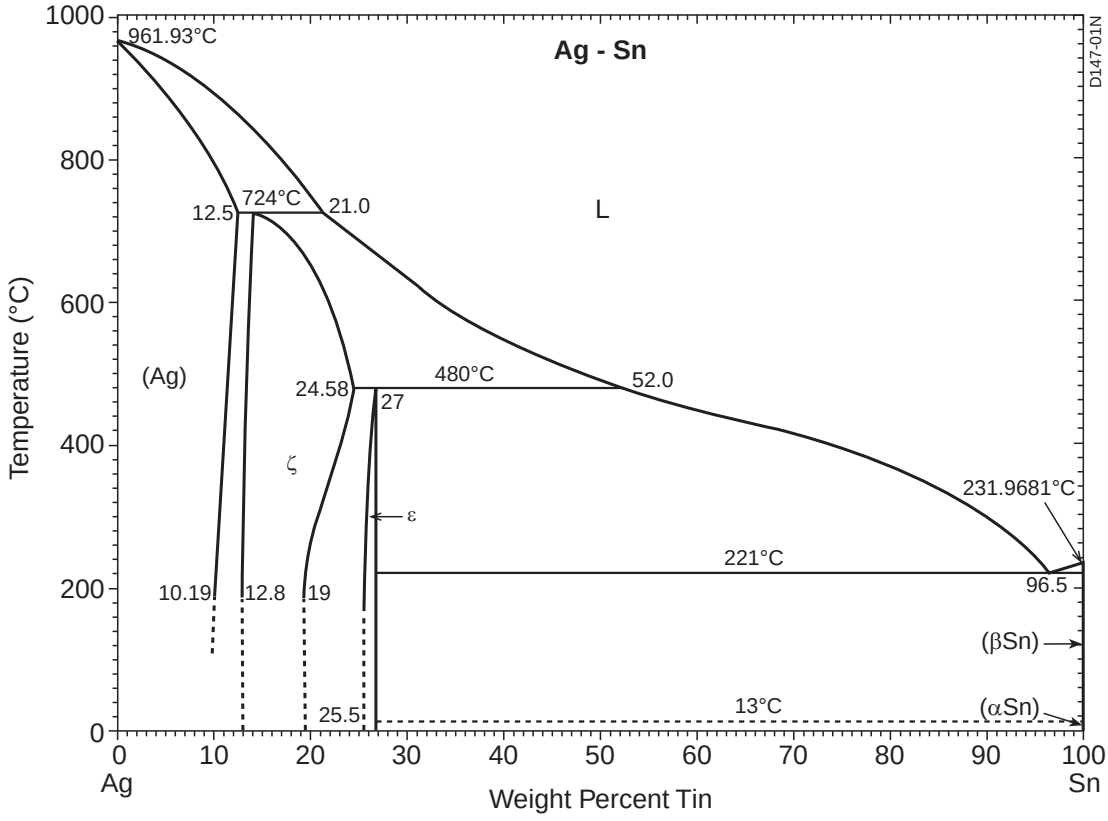
Ag - Sn
D147-01N
Temperature (°C)
Weight Percent Tin
Ag
Sn
961.93°C
L
724°C
12.5
21.0
(Ag)
480°C
24.58
52.0
27
ζ
ε
231.9681°C
221°C
96.5
10.19
12.8
19
(βSn)
25.5
13°C
(αSn)

A.3.3 Alloying elements with maximum primary solid solubilities above eutectic temperatures

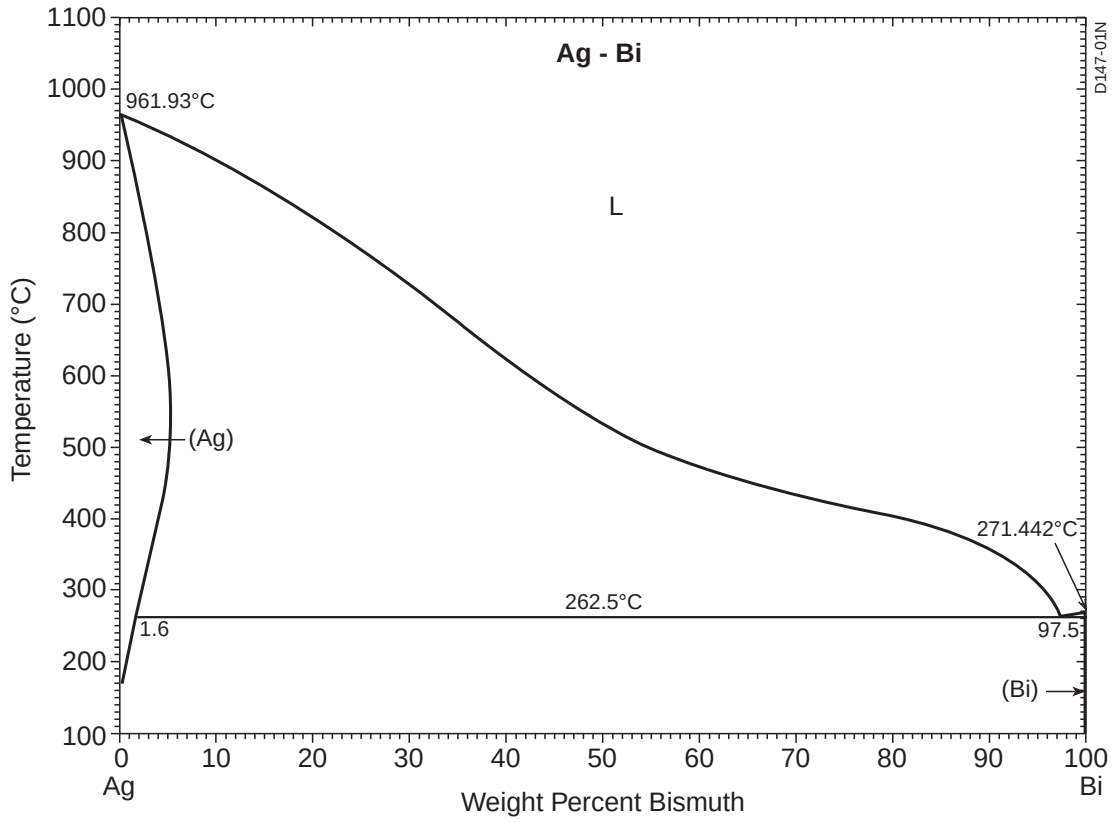

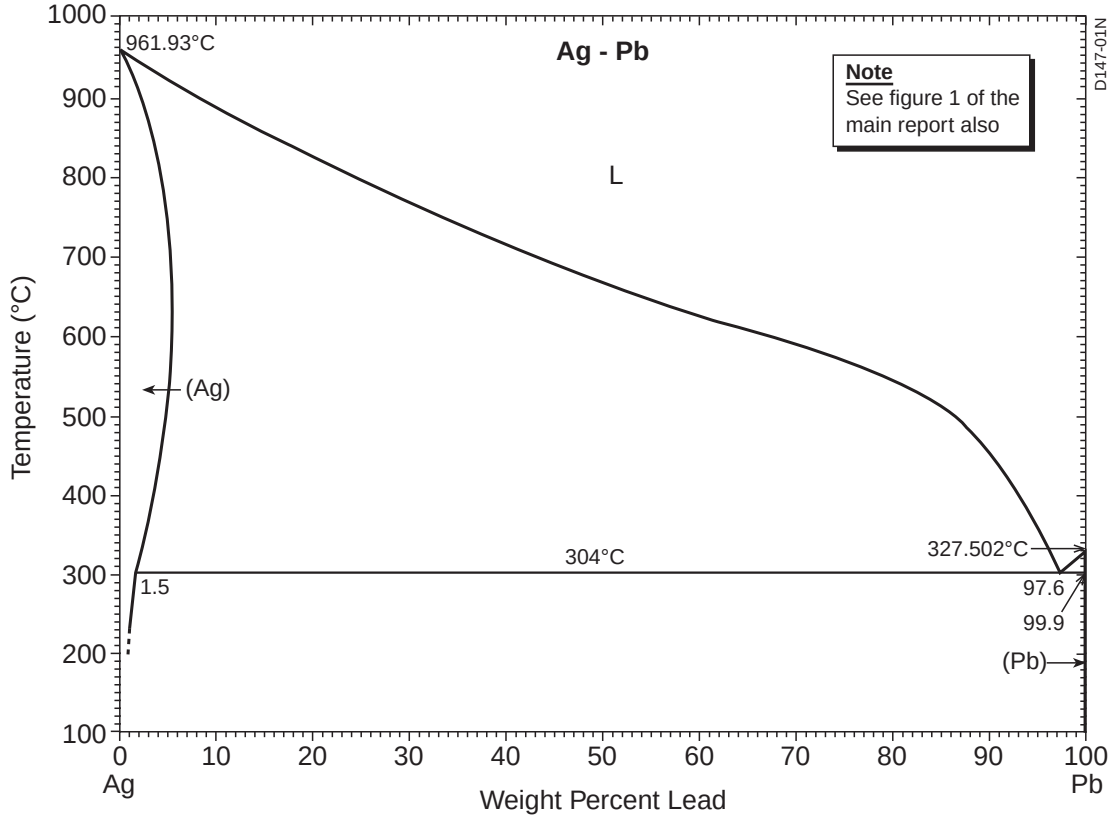

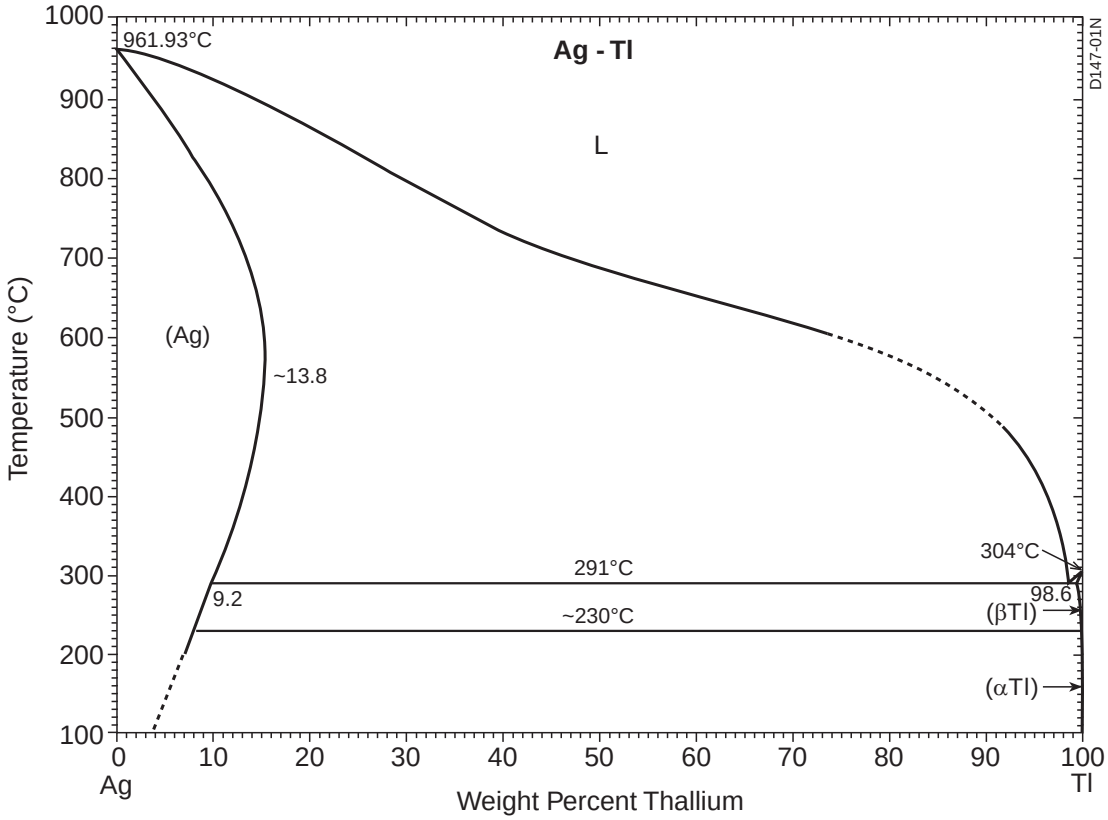
Ag - Tl
961.93°C
L
(Ag)
~13.8
9.2
291°C
304°C
98.6
~230°C
(βTl)
(αTl)
Temperature (°C)
Weight Percent Thallium
Ag
Tl
D147-01N

Appendix B Classification of archaeological silver artifacts and coins in support of figure 11

B.1 Table B.1: artifacts

Table B.1 Classification and weight % of actually and potentially embrittling impurity elements in archaeological silver artifacts

85 ≤ Ag wt.% < 95								95 ≤ Ag wt.%								REFERENCES AND COMMENTS
Pb	Bi	Sb	Sn	Pb	Bi	Sb	Sn	Pb	Bi	Sb	Sn	Pb	Bi	Sb	Sn	
0.2 0.5								0.2 0.4				0.3				Lucas (1928)
0.2 0.2 1.6 0.2 0.2	0.19 0.18 0.19 			0.2 0.5 0.4 0.2 0.71				0.5 0.2 0.5 0.2 0.1	 0.19 0.19 			0.1 0.5 				Gale and Stos-Gale (1981a). One outlier (2.9 wt.% Pb; 1.5 wt.% Bi) excluded
1.68 1.65 1.10 1.15 0.71 0.90 0.73 0.81 1.18 0.53 1.05 1.04 0.91	<0.01 <0.01 <0.01 0.18 0.22 0.04 0.05 0.07 0.06 0.04 0.08 0.03 0.07	<0.10 0.10 0.08 0.33 0.21 0.21 0.22 0.21 0.17 0.15 0.23 0.50 0.21	^ <0.1 v					0.42 0.39 0.56 0.50 0.43 0.44 0.45 0.41 0.22 0.97 0.18 0.16 0.16 0.25 0.46	0.19 0.15 <0.01 <0.01 0.06 0.05 <0.01 <0.01 0.21 <0.01 0.16 0.17 0.26 <0.01 0.07	<0.10 0.20 <0.10 <0.10 <0.10 0.14 0.15 0.18 0.10 0.15 0.15 0.13 0.18 <0.1 <0.10	^ <0.1 v	0.30 0.25 0.06 0.45 0.46 0.43 2.70 0.84 0.53 1.17 1.08 0.46 0.44 0.22	<0.01 <0.01 0.15 0.10 <0.01 <0.01 0.15 <0.01 0.04 0.05 0.07 0.03 0.02 <0.01	<0.10 0.18 <0.10 <0.10 0.11 0.35 <0.10 0.40 <0.10 0.44 0.20 <0.10 0.14 0.23	^ <0.1 v	Bennett (1994). All analyses: less than 0.1 wt.% Sn and less than 0.005 wt.% As
85 ≤ Ag wt.% < 95												0.7 1.1 0.6 0.9 0.1 0.2 0.3 0.2 0.2 0.2 0.7				0.014 0.014 0.005 0.007 0.005 0.036	Perea and Rovira (1995).One analysis for 85 ≤ Ag wt%<95 gave 0.15 wt.% Sb
Pb	Sn	Pb	Sn	Pb	Sn	Pb	Sn	Pb	Sn	Pb	Sn					
0.8 0.3 0.4 0.7 0.6 1.3 0.5 0.6 0.6	0.385 0.022 0.063 0.228 0.340	0.3 1.0 0.5 0.8 0.4 0.4 0.2 0.2 1.9	 0.043 0.024 0.024 0.052	0.6 1.2 1.7 0.8 0.7 0.6 1.7 3.4 2.4	0.129 0.013 0.19 0.092 	2.0 1.0 1.0 0.6 1.4 0.4 0.2 1.0 0.2	 0.073 0.018 0.267 0.018 0.006	0.8 1.5 0.2 0.4 0.3 0.4 0.4 0.5 0.3	0.003 0.185 0.012 0.233 0.016 0.035 0.032	1.2 0.7 1.3 1.7	0.051					

Table B.2 Classification and weight % of actually and potentially embrittling impurity elements in archaeological silver coins

85 ≤ Ag wt.% < 95								95 ≤ Ag wt.%								REFERENCES AND COMMENTS
Pb	Sn	Pb	Sn	Pb	Sn	Pb	Sn	Pb	Sn	Pb	Sn	Pb	Sn	Pb	Sn	
0.57	0.17	0.88		0.85	0.08	0.23	0.02	0.46		2.19		0.72	0.06	3.68		Caley (1964)
1.09	0.02	0.47		0.63	0.08	0.25	0.04	0.63		0.85		2.87		0.13		
1.22	0.04	0.37	0.26	0.39	0.17			1.03		0.86		3.05		0.43		
0.39	0.23															Tylecote (1992)
0.38		1.05		0.44				0.25								Cope (1972)
0.37		0.78		1.02												
0.95		0.34		0.61												
0.5		0.2						0.3		0.2		0.6				MacDowall (1972)
0.6		4.7						0.7		0.7						
1.58	0.05	1.48	0.10	1.10	0.05			0.68	0.07	1.10	0.01					Gordus (1972)
1.85	0.12	1.63	0.10					0.42	0.10							
	0.4		0.1		0.8	0.2										Metcalf (1972)
	0.9		0.5		0.3	0.3										
	1.4		0.7		0.6											
	0.5		0.8		0.1											

85 ≤ Ag wt.% < 95															95 ≤ Ag wt.%			
Pb	Bi	Sn	Pb	Bi	Sn	Pb	Bi	Sn	Pb	Bi	Sn	Pb	Bi	Sn	Pb	Bi	Sn	
1.5	0.0	2.9	1.0	0.0		1.2	0.0	0.5	1.3	0.1	0.8	1.7	0.0	0.0	0.1		0.0	McKerrell and Stevenson (1972). One outlier (0.6 wt.% Pb; 8.7 wt.% Bi; 0 wt.% Sn) excluded
2.4	0.2	1.7	2.8	0.2	0.5	1.4	0.1	0.2	1.1	0.2	0.9	1.1	0.0		0.7		0.0	
2.5	0.0	0.2	1.1	0.0	0.0	0.9	0.1	0.6	1.3	0.0	0.0	1.4	0.1		1.0	0.1		
2.0	0.0	0.0	0.6	0.2	0.5	1.1	0.2	0.2	1.2	0.2	0.3	1.6	0.2	0.4	1.0			
1.1	0.1	0.1	0.8	0.1	0.2	1.4	0.0		1.6	0.1	0.7	1.4	0.3	0.2	0.5	1.3	0.0	
1.7	0.1	0.2	1.4	0.2	0.3	1.3	0.2	0.3	1.6	0.0		1.7	0.0		0.6	0.3	0.0	
0.9	0.0	0.1	0.9	0.2		1.2	0.0	0.2	1.2	0.1		1.2	0.3		0.6	0.4	0.0	
1.4	0.1	0.3	1.6	0.1		0.9	0.0	0.2	1.9	0.0		1.4	0.2	0.3	0.9	0.2	0.0	
0.7	0.0	0.3	1.3	0.0	0.2	1.4	0.3	0.5	0.8	0.1	0.3	1.3	0.1	0.1	0.6	0.2	0.0	
1.3	0.2	0.5	0.8	0.0		1.2	0.1	0.3	1.4	0.2	0.6	1.3	0.0		0.4	1.0	0.0	
0.9	0.1	0.6	1.3	0.0	0.1	1.2	0.2	0.6	1.3	0.2	0.0	1.9	0.0		0.3	0.7	0.0	
1.2	0.2	0.3	1.2	0.1	1.0	1.0	0.0	0.4	1.4	0.0		1.1	0.0		0.9	0.2	0.0	
0.7	0.0	0.1	1.2	0.0	0.4	1.3	0.3	0.9	1.8	0.1	0.5	0.9	0.0		0.3	1.3	0.0	
1.0	0.1	0.3	1.9	0.3	0.2	1.3	0.2	0.3	1.4	0.2	0.2	1.2	0.2	0.0	0.2	0.5	0.0	
0.8	0.0	0.0	0.9	0.1	0.3	0.9	0.1		1.4	0.1	0.1	1.0	0.0	0.2				
1.4	0.1	0.3	1.4	0.2	0.6	1.6	0.2		2.0	0.2	0.5	1.0	1.2	0.0				
1.0	0.0	0.0	0.6	0.1	0.2	2.6	0.2	0.3	1.3	0.0	0.0	0.9	1.3	0.0				
0.9	0.1	0.3	1.0	0.1	0.4	2.5	0.1		1.4	0.2		0.7	0.8	0.2				
1.1	0.0		1.1	0.2	0.5	1.5	0.0		1.3	0.0								

Appendix C Description of corrosion-induced embrittlement of archaeological silver

C.1 Types of corrosion

Figure C.1 shows the types of corrosion observed for archaeological silver. The examples are a Roman cup (Werner 1965), a late Roman plate (Bennett 1994), a Sican tumi (Scott 1996) and an Egyptian vase (Wanhill *et al*. 1998).

General corrosion is slow conversion of the metal surface to silver chloride (Gowland 1918; Scott 1996). This forms a brittle, finely granular layer but does not affect the remaining metal's integrity. However, unfavourable conditions may result in an artifact being completely converted to silver chloride, sometimes retaining its shape, sometimes not (Gowland 1918).

The other types of corrosion penetrate the metal. Cracking along the corrosion paths reduces an artifact's resistance to fragmentation (Werner 1965; Ravich 1993; Wanhill *et al*. 1998). Intergranular corrosion can occur in mechanically worked and annealed artifacts. Interdendritic corrosion can occur in castings with essentially as-cast microstructures, i.e. little changed by any subsequent mechanical working or annealing, see Scott (1996). Corrosion along slip lines and deformation twin boundaries can occur in an artifact that has not been annealed after final mechanical working, which includes chased and stamped decorations (Wanhill *et al*. 1998): inside the metal these types of attack can lead to additional corrosion along segregation bands. These bands are the remains, modified by mechanical working and annealing heat-treatments, of solute element segregation (coring) and interdendritic segregation that occurred during solidification of an ingot or cupelled button.

Cracking along the corrosion paths in the metal usually results in irregular fracture surfaces with a finely granular appearance like that of the general corrosion in the upper fractograph of figure C.1. However, highly localised corrosion along slip lines and deformation twin boundaries results in crystallographic fractures, for example the lower fractograph in figure C.1.

C.2 Synergistic action of corrosion-induced and microstructurally-induced embrittlement

Corrosion-induced and microstructurally-induced embrittlement can act synergistically (Wanhill 2000a; Wanhill *et al*. 1998). Figure C.2 gives examples of the appearances of synergistic embrittlement. Corrosion along slip lines, deformation twin boundaries and segregation bands can result in cracks under the action of external loads or forces (e.g. crushing pressures during interment) and internal residual stresses due to retained cold-work. These cracks can then

initiate fracture along microstructurally-embrittled grain boundaries – which may fracture anyway under the action of external loads or forces, see the discussion section in the main part of this report. In turn, grain boundary fractures expose more slip lines, deformation twins and segregation bands to the environment and therefore increase the opportunities for corrosion.

C.3 Mechanisms of corrosion-induced embrittlement

Intergranular corrosion has been attributed, at least partly, to segregation of the solute element copper to grain boundaries (Werner 1965; Ravich 1993). This segregation is of a type called cellular (or discontinuous) precipitation. It occurs in the solid state at temperatures as low as 150°-200 °C (Scharfenberger *et al*. 1972; Gust *et al*. 1978; Schweizer and Meyers 1978) and could occur very slowly even at ambient temperatures (Schweizer and Meyers 1978). Besides temperature, the precipitation rate depends strongly on the solute element (copper) content of the metal and the amount of plastic deformation (cold-work) retained in the microstructure (Hornbogen 1972; Pawlowski 1979a, 1979b): lower solute contents reduce the precipitation rate, plastic deformation increases it.

The actual mechanism of intergranular corrosion is localised galvanic attack, whereby in the presence of a moisture-containing environment the more noble metal (in this case the copper-depleted silver matrix) acts as a cathode and the copper-enriched grain boundary region dissolves anodically.

The other two types of segregation-induced corrosion, interdendritic and along segregation bands that are the remains of coring and interdendritic segregation, are also due to solute element (copper) segregation which, however, occurs at high temperatures during solidification of the metal. In both cases the corrosion mechanism is most likely the same as for intergranular corrosion, i.e. localised galvanic attack of the less noble copper-enriched regions.

It remains to discuss corrosion along slip lines and deformation twin boundaries, firstly in a general way. Slip, which occurs in bands, and deformation twinning involve locally high strains whereby some atoms are in non-equilibrium positions and have higher energies: in slip bands the atoms surrounding dislocation cores, and in deformation twins the atoms in noncoherent regions of the twin/matrix interfaces. When slip bands and deformation twin boundaries are surface-connected, as in the archaeological silver examples in figure C.2, these higher energy regions are susceptible to preferential corrosion (e.g. Procter 1994, 1:37). Note that the annealing twin boundaries in figure C.2 are uncorroded. Apparently, the local environmental conditions were not severe enough to cause preferential corrosion at these twin/matrix interfaces, which by nature are coherent and without highly strained regions.

More specifically, for silver there are additional factors that could promote corrosion along slip lines and deformation twin boundaries. These are silver's low stacking fault energy* (Hertzberg 1983, 80, 129) which results in planar slip and hence greater concentrations of dislocations in slip bands; the narrowness of the deformation twins, e.g. figure C.2, which means higher local strains (Hertzberg 1983, 111); and for archaeological silver the possibility of long-term segregration of solute and impurity elements to the highly strained regions, thereby aiding preferential corrosion (Procter 1994, 1:39).

* In metals having crystal structures with close-packed atomic arrangements, including silver, the slip plane dislocations can dissociate to form two partial dislocations bounding a stacking fault, which is a local "error" in the atomic arrangement. The lower the stacking fault energy, the wider the stacking fault, and the more difficult it is to recombine the partial dislocations to allow them to glide onto other slip planes (so-called wavy slip behaviour). Consequently, a low stacking fault energy favours dislocation movement being restricted to the original slip plane (so-called planar slip behaviour).

General (surficial) corrosion

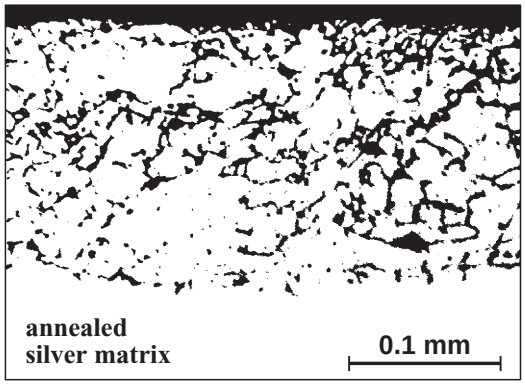

Metallograph (Bennett 1994)

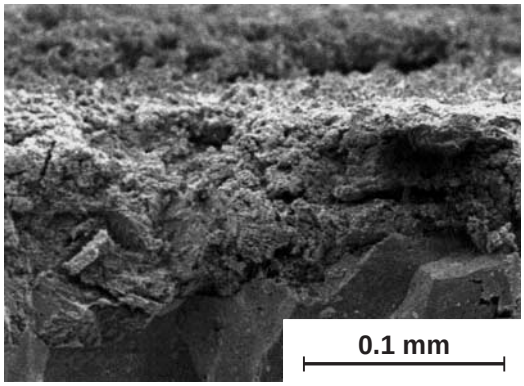

SEM fractograph (Wanhill *et al.* 1995)

Intergranular or interdendritic corrosion

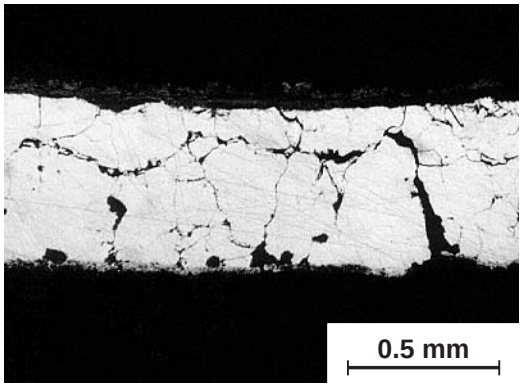

Intergranular: metallograph (Werner 1965)

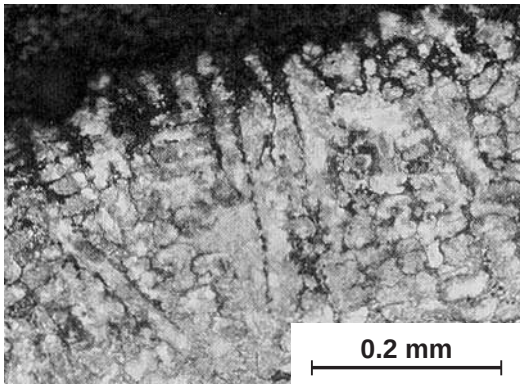

Interdendritic: metallograph (Scott 1996)

Slip line, deformation twin boundary and segregation band corrosion

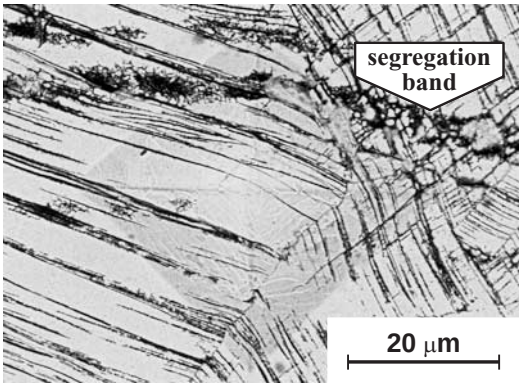

Corrosion along slip lines, deformation twins and segregation bands: SEM metallograph (Wanhill *et al.* 1998)

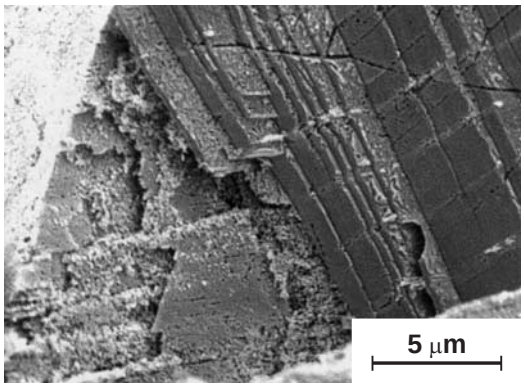

Crystallographic fracture owing to corrosion along slip lines and deformation twins: SEM fractograph (Wanhill *et al.* 1998)

Fig. C.1 Types of corrosion of archaeological silver: SEM = Scanning Electron Microscopy

Synergistic embrittlement

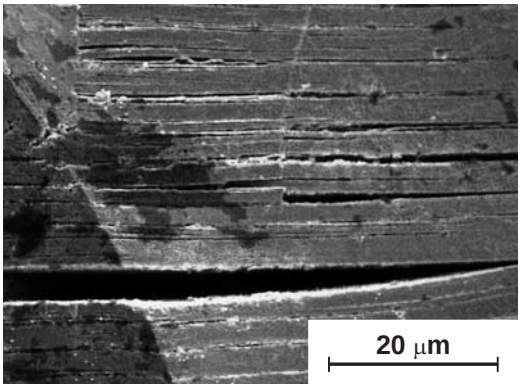

Corrosion along slip lines intersecting grain boundary facets: SEM fractograph (Wanhill *et al*. 1998)

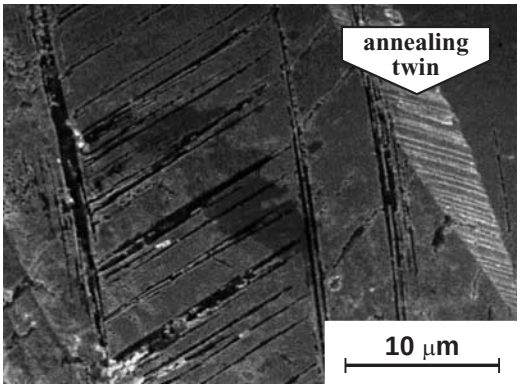

Corrosion along deformation twin boundaries intersecting a grain boundary facet: SEM fractograph (Wanhill *et al*. 1998)

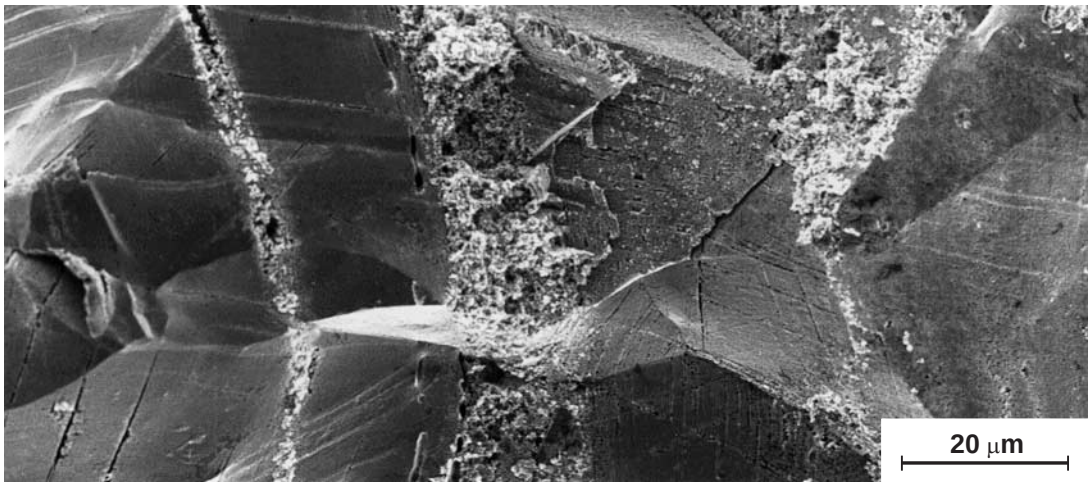

Corrosion along segregation bands intersecting grain boundary facets: SEM fractograph (Wanhill *et al*. 1998)

Fig. C.2 Examples of synergistic embrittlement owing to microstructurally-induced embrittlement (intergranular fracture) and corrosion-induced embrittlement along slip lines, deformation twin boundaries and segregation bands